

KiDS-Legacy: The consistency test of the large-scale structure with Bernardeau-Nishimichi-Taruya transform

Shiming Gu (顾时铭)^{1,2,*} Ziang Yan (颜子昂)^{2,3,4,†} Ludovic van Waerbeke^{1,‡} Francis Bernardeau^{5,6}
 Hendrik Hildebrandt² Angus H. Wright² Maciej Bilicki⁷ Christos Georgiou⁸ Shun-Sheng Li (李
 顺生)^{9,10} Laila Linke¹¹ Lauro Moscardini^{12,13,14} Robert Reischke^{15,2} and Benjamin Stözlner²

¹*Department of Physics & Astronomy, University of British Columbia, 6224 Agricultural Road, Vancouver, BC V6T 1Z1, Canada*

²*German Centre for Cosmological Lensing, Astronomisches Institut, Ruhr-Universität Bochum, Universitätsstr. 150, 44780, Bochum, Germany*

³*Graduate School of Science, Nagoya University, Furocho, Chikusa-ku, Nagoya, Aichi, 464-8602, Japan*

⁴*Kobayashi-Maskawa Institute for the Origin of Particles and the Universe (KMI), Nagoya University, Nagoya, 464-8602, Japan*

⁵*Université Paris-Saclay, IPHT, DRF-INP, UMR 3681, CEA, Orme des Merisiers Bat 774, 91191 Gif-sur-Yvette, France*

⁶*Center for Gravitational Physics and Quantum Information, Yukawa*

Institute for Theoretical Physics, Kyoto University, Kyoto 606-8502, Japan

⁷*Center for Theoretical Physics, Polish Academy of Sciences, al. Lotników 32/46, 02-668 Warsaw, Poland*

⁸*Institut de Física d'Altes Energies (IFAE), The Barcelona Institute of Science and Technology, Campus UAB, 08193 Bellaterra (Barcelona), Spain*

⁹*Kavli Institute for Particle Astrophysics and Cosmology, Stanford University, Stanford, CA 94305, USA*

¹⁰*SLAC National Accelerator Laboratory, Menlo Park, CA 94025, USA*

¹¹*Universität Innsbruck, Institut für Astro- und Teilchenphysik, Technikerstr. 25/8, 6020 Innsbruck, Austria*

¹²*Dipartimento di Fisica e Astronomia 'Augusto Righi' - Alma Mater Studiorum*

Università di Bologna, via Piero Gobetti 93/2, I-40129 Bologna, Italy

¹³*Istituto Nazionale di Astrofisica (INAF) - Osservatorio di Astrofisica e*

Scienza dello Spazio (OAS), via Piero Gobetti 93/3, I-40129 Bologna, Italy

¹⁴*Istituto Nazionale di Fisica Nucleare (INFN) - Sezione di Bologna, viale Berti Pichat 6/2, I-40127 Bologna, Italy*

¹⁵*Argelander-Institut für Astronomie, Universität Bonn, Auf dem Hügel 71, D-53121 Bonn, Germany*

(Dated: July 7, 2026)

We perform the first k -cut cosmic shear analysis of the KiDS-Legacy survey. This method uses the Bernardeau-Nishimichi-Taruya (BNT) transform to construct weak-lensing kernels that are more localised than conventional ones, and remove information from selected physical scales while retaining the constraining power of the targeted range. Removing the scale of $k \geq 0.33 \text{ Mpc}^{-1}$ from the KiDS-Legacy pseudo- C_ℓ data vector, and using a covariance matrix whose Gaussian component is computed from the theoretical data vector, we find $S_8 = 0.798^{+0.045}_{-0.045}$. This agrees with both the fiducial KiDS-Legacy bandpower result and our no- k -cut pseudo- C_ℓ posterior to within 0.1σ , indicating no significant bias from nonlinear astrophysical feedback at the precision of KiDS-Legacy. We also study the case in which the Gaussian covariance is computed from the observed data vector. In this setup, the same scale cut of $k < 0.33 \text{ Mpc}^{-1}$ gives a much lower $S_8 = 0.717^{+0.047}_{-0.046}$. Further k -cut tests reveal a mild scale-dependent trend, with larger physical scales preferring lower S_8 values and a maximum low- versus high- k deviation of 1.80σ . Mock tests show that this behaviour is not produced by the covariance prescription or data vector alone, but may arise from their interplay. These results show that BNT k -cuts provide both a mitigation strategy for nonlinear systematics and a diagnostic of weak-lensing inference pipelines.

I. INTRODUCTION

Since the late-20th century, the Λ CDM framework has emerged from a set of partly independent empirical clues into the concordance model of cosmology. Cold dark matter (CDM) was proposed in the 1980s to explain the formation of galaxies and large-scale structure [1], and it quickly became a working framework once N-body and semi-analytic calculations demonstrated that a collisionless, non-relativistic dark matter component could repro-

duce the observed clustering properties [2, 3]. At the same time, these clustering measurements indicated that the matter density Ω_m of the Universe was less than about half of the critical density [4, 5]. In contrast, inflationary theory and CMB measurements favoured a spatially flat geometry, which requires the total matter-energy density to be very close to the critical value [6–8]. This tension motivated a renewed consideration of Einstein’s cosmological constant term Λ [9] as a possible resolution [10, 11]. The idea provided a bridge between otherwise conflicting observations and was soon strongly supported when Type Ia supernova measurements revealed that the cosmic expansion is accelerating. With this convergence of theoretical and observational evidence, the modern standard model of cosmol-

* gsm@phas.ubc.ca

† yan.ziang.h1@f.mail.nagoya-u.ac.jp

‡ waerbeke@phas.ubc.ca

ogy, Λ CDM, took shape, offering a remarkably successful description of a wide range of cosmological phenomena.

Since the discovery of cosmic acceleration via the so-called “standard candle” – Type Ia supernovae, a variety of observational probes have been developed or further refined to test and constrain the Λ CDM model across different cosmic epochs and scales. Analogous to standard candles, standard rulers such as baryon acoustic oscillations [BAO, 12] measured in large galaxy redshift surveys [13, 14] provide robust distance measurements that further test the Λ CDM framework. At intermediate redshifts, the abundance and spatial distribution of galaxy clusters detected through different methods, including the Sunyaev-Zel’dovich [SZ effect, 15], offer valuable constraints on the growth of structure and the matter content of the Universe. The most precise cosmological measurements to date come from cosmic microwave background (CMB) anisotropies [7, 16], which impose tight constraints on the initial conditions and geometry of the Universe. Collectively, these diverse datasets represent the current state of the art in testing the Λ CDM model, demonstrating remarkable consistency while revealing important tensions – sometimes referred to as the new ‘Kelvin’s Clouds’ of cosmology – most notably the discrepancies in measurements [17, 18] of the Hubble parameter [H_0 tension, 19] and the amplitude of matter fluctuations [S_8 tension, 20].

The so-called S_8 parameter, defined as $S_8 = \sigma_8(\Omega_m/0.3)^{0.5}$, where σ_8 is the amplitude of density fluctuations in the universe on a scale of 8 Mpc/ h and Ω_m , plays a central role in quantifying the amplitude of matter fluctuations relevant for late-time structure formation. Many of the measurements of late-time S_8 come from studies of weak gravitational lensing, which probe subtle, coherent distortions in the shapes of distant galaxies induced by intervening large-scale mass distributions. Since these shape distortions are individually too small to be detected, weak lensing relies on statistical analyses [21–24] of correlated shape changes across large galaxy samples [25, 26]. This technique, called *cosmic shear*, has matured into a powerful cosmological probe, offering direct insight into the distribution and growth of matter, and enabling stringent tests of dark matter and dark energy models [27]. In recent years, a growing number of large imaging surveys have employed weak lensing to map the matter density field with unprecedented precision. These measurements have revealed tensions in the inferred value of S_8 when compared to predictions from the cosmic microwave background under the Λ CDM model, which could point to gaps in our current understanding of cosmology.

Building on these developments, the Kilo-Degree Survey (KiDS) [28] has emerged as one of the leading weak-lensing programmes designed to probe S_8 with high precision. Conducted with the VLT Survey Telescope (VST) and its 268-megapixel OmegaCAM imaging device [29], KiDS delivers superb, uniform image quality over a $1^\circ \times 1^\circ$ field, enabling precise shape measurements

essential for cosmic shear analyses. Its technical foundations – including the Astro-WISE data system [30], multi-band photometry, and the lensfit Bayesian shear measurement algorithm [31] – provide robust photometric redshifts, stringent control of systematics, and statistically powerful lensing catalogues. Using these tools, the KiDS-1000 analysis reported a relatively low clustering amplitude, $S_8 = 0.759^{+0.024}_{-0.021}$, corresponding to a $\sim 3\sigma$ offset from Planck CMB predictions in simple S_8 comparisons [32]. However, the most recent KiDS-Legacy cosmic shear results [33, 34], based on the full survey footprint and improved photometric redshift estimation, yield $S_8 = 0.813^{+0.018}_{-0.018}$ (COSEBIs Marginal Mean + CI)¹, consistent with Planck at the 0.73σ level, illustrating how expanded datasets and, more importantly, a different methodology can materially change the inferred level of tension.

In addition to uncertainties in photometric redshifts, one of the most widely discussed explanations for the S_8 tension involves effects in the modelling of the nonlinear regime [35]. Within the standard theory of cosmic structure growth, linear scales are expected to retain detectable information about both the cosmic expansion history and the matter content established before recombination [36]. It is therefore necessary to investigate nonlinear scales or late-time growth, which are more susceptible to physical processes that are less well understood than linear evolution. Such processes include unexpected strong baryonic feedback [37, 38], late-time scalar fields [39, 40], and exotic dark matter models [41, 42]. However, these explanations typically require either non-minimal extensions of the standard cosmological model or baryonic feedback strengths that are disfavoured by independent astronomical constraints [43]. As a result, despite their ability to improve the fit to certain observational datasets, these alternatives are disfavoured under Occam’s razor principle, compared to the standard Λ CDM model.

However, even if such models could explain why weak lensing measurements yield a lower S_8 value, they generally affect the cosmic large-scale structure differently than changes in standard cosmological parameters such as the matter density Ω_m and the scalar fluctuation amplitude A_s . For example, some models recover the Planck S_8 by suppressing power in the nonlinear regime [35, 37]. Weak lensing, however, traces all matter along the line of sight, so correlations measured at given angular scales receive contributions from a wide range of physical scales. This well-known projection effect limits the effectiveness of nonlinear corrections. To address this limitation, the Bernardeau–Nishimichi–Taruya (BNT) transform [44] was proposed. The BNT effectively localises

¹ Please note that the official KiDS-Legacy cosmic shear paper quoted the fiducial COSEBIs result as their main result. However, as we are using pseudo- C_ℓ , whose data vector structure is closer to the bandpowers, we will mostly quote their bandpower results $S_8 = 0.797^{+0.023}_{-0.024}$ in this paper.

cosmic shear tomography to a narrower redshift range, and when combined with a well-defined angular-scale filter (ℓ -cut in harmonic space), it can nearly serve as a 3-D physical-scale cut in Fourier space. This enables more robust mitigation of uncertainties associated with nonlinear modelling of the three-dimensional matter power spectrum. In our previous works [42, 45], we developed a BNT-based cosmic shear analysis pipeline, demonstrated that the BNT transform can serve as a targeted solution for nonlinear systematics, and proposed a BNT-based consistency test for modelling uncertainties within the posterior sampling process.

From the comparison of Taylor *et al.* [46] and Gu *et al.* [42], we also find that it is much better to use BNT transform in the harmonic ℓ -space rather than the configuration space to target the k -cut information more effectively. However, it is generally challenging to calculate C_ℓ on the weighted sky (for example, partially covered sky with anisotropic lensing weights). The KiDS cosmic shear analyses [32, 33] use the bandpower, that is, measuring real-space correlation functions first, then transferring to ℓ -space with pre-defined bandpower window functions. In this work, we use the pseudo- C_ℓ method [PCL, 47], that is, directly taking harmonic transformation from the weighted shear maps, then correcting for the mode-coupling induced by the weights. Compared to catalogue-based correlation functions, this method is relatively faster, especially when estimating the covariance [48]. In addition, one can make cleaner scale cuts with pseudo- C_ℓ .

The structure of the paper is organised as follows. In Section II, we introduce the theoretical foundations of weak gravitational lensing, pseudo- C_ℓ estimators, and the BNT transform. In Section III, we describe the data, the construction and manipulation of the data vector, the modelling procedure, and the pipeline for inferring cosmological parameters from the observables. In Section IV, we present BNT-based S_8 constraints derived from different physical scale selections and discuss their cosmological implications. Finally, Section V summarises our findings and provides concluding remarks.

II. THEORETICAL MODELLING

A. Power Spectra

The information properties of the cosmic large-scale structure are often described by its two-point statistics. At the second order, the matter density field is usually characterised by the power spectrum $P(k; z)$:

$$\langle \delta(\mathbf{k}; z) \delta^*(\mathbf{k}'; z) \rangle = (2\pi)^3 \delta_D(\mathbf{k} - \mathbf{k}') P(k; z). \quad (1)$$

where δ_D is the Dirac delta function. In weak lensing observation, we probe projected fields rather than a full 3D matter distribution. The cosmic shear signal traces the integrated matter fluctuations along the line of sight,

with its corresponding observable, the cosmic shear angular power spectrum C_ℓ , which can be decomposed to the contribution of the cosmic shear, galaxy intrinsic shape (or intrinsic alignment, IA), and their cross-correlations:

$$C^{i,j} \equiv C_{\text{GG}}^{i,j} + C_{\text{GI}}^{i,j} + C_{\text{IG}}^{i,j} + C_{\text{II}}^{i,j}. \quad (2)$$

The shear-shear component, $C_{\text{GG}}^{i,j}$ is related to $P(k; z)$ through a line-of-sight projection weighted by the lensing efficiency and geometry [49]:

$$C_{\text{GG}}^{i,j}(\ell) = \int \frac{d\chi}{f_K(\chi)^2} W_\gamma^i(\chi) W_\gamma^j(\chi) P\left(k = \frac{\ell + 1/2}{\chi}; z(\chi)\right); \quad (3)$$

where χ is the radial comoving distance, $f_K(\chi)$ is the angular diameter distance at χ^2 :

$$f_K(\chi) = \begin{cases} \frac{1}{\sqrt{K}} \sin(\sqrt{K} \chi), & K > 0 \text{ (closed)}, \\ \chi, & K = 0 \text{ (flat)}, \\ \frac{1}{\sqrt{-K}} \sinh(\sqrt{-K} \chi), & K < 0 \text{ (open)}, \end{cases} \quad (4)$$

and $W_\gamma^i(\chi)$ is the lensing kernel computed by the source redshift distribution of the i^{th} tomographic bin of a given survey:

$$W_\gamma^i(\chi) = \frac{3\Omega_m H_0^2}{2c^2} \int d\chi' \frac{n_i(\chi')}{a(\chi')} \frac{f_K(\chi' - \chi) f_K(\chi)}{f_K(\chi')}, \quad (5)$$

where $n_i(\chi(z))$ is the redshift distribution of galaxies.

In this paper, we use the nonlinear alignment model [NLA, 50] to model the intrinsic correlation of the galaxy shapes. It can be described by applying a redshift-dependent linear bias $C_1(z)$ to the nonlinear matter power spectrum:

$$\begin{aligned} P_{\text{GI}}(k, z) &= C_1(z) P_{\text{nl}}(k; z) \\ P_{\text{II}}(k, z) &= C_1^2(z) P_{\text{nl}}(k, z) \end{aligned} \quad (6)$$

where the tidal alignment bias $C_1(z)$ is always parameterised as a redshift-dependent function involving a global IA scaling amplitude A_{TA} and a power-law evolution index η_{TA} where we use $\eta_{\text{TA}} = 0$ in this paper in order to be consistent with the parameter choice of [33]:

$$C_1(z) \equiv -A_{\text{TA}} \tilde{C}_1 \frac{\rho_{\text{crit}} \Omega_m}{D(z)} \left(\frac{1+z}{1+z_0} \right)^{\eta_{\text{TA}}} \quad (7)$$

where ρ_{crit} is the critical density of the universe, $D(z)$ is the structure growth function, z_0 is a pivot redshift fixed to $z_0 = 0.62$ [51], and $\tilde{C}_1 = 5 \times 10^{-14} h^{-2} \text{M}_\odot^{-1} \text{Mpc}^3$ is a normalisation constant. The corresponding angular power spectra of the intrinsic alignment can be expressed

² Throughout the paper, we assume a spatially flat Universe with zero spatial curvature, $K = 0$

as line-of-sight integrals of the three-dimensional power spectra P_{GI} and P_{II} :

$$C_{\text{GI}}^{i,j}(\ell) = \int \frac{d\chi}{f_K(\chi)^2} W_\gamma^i(\chi) W_N^j(\chi) P_{\text{GI}}(k; z) \quad (8)$$

$$C_{\text{IG}}^{i,j}(\ell) = \int \frac{d\chi}{f_K(\chi)^2} W_N^i(\chi) W_\gamma^j(\chi) P_{\text{GI}}(k; z) \quad (9)$$

$$C_{\text{II}}^{i,j}(\ell) = \int \frac{d\chi}{f_K(\chi)^2} W_N^i(\chi) W_N^j(\chi) P_{\text{II}}(k; z) \quad (10)$$

where $W_N^i(\chi)$ is the number density projection kernel:

$$W_N^i(\chi) = \frac{H(\chi)}{c} n_i(z(\chi)), \quad (11)$$

where $H(\chi)$ is the Hubble parameter at χ .

To account for the sky weight induced by the footprint and lensing weights, we employ the pseudo- C_ℓ method [PCL, 52] to estimate the angular power spectra of cross-correlations. This will be introduced in Section III.

B. BNT Transform

BNT transform aims to reorganise the data vector $C^{i,j}(\ell)$ to a new $\hat{C}^{a,b}(\ell)$, where a and b represent the set of linear combinations of the original tomographic redshift bins i and j . Throughout the paper, we use the ‘hat’ notation $\hat{\cdot}$ for all BNT transformed quantities, and reserve the use of (i, j) for the ordinary, noBNT tomographic bins while using (a, b) for the BNT tomographic bins.

To compute the BNT transform matrix p_i^a , we need two normalisation numbers n_i^0 and n_i^1 for each tomographic bin i :

$$n_i^0 = \int d\chi n_i(\chi) \quad (12)$$

$$n_i^1 = \int d\chi \frac{n_i(\chi)}{\chi} \quad (13)$$

so we can construct the following algebraic equations:

$$\sum_{i=a-2}^a p_i^a n_i^0 = 0 \quad (14)$$

$$\sum_{i=a-2}^a p_i^a n_i^1 = 0, \quad (15)$$

with $p_i^a = 0$ when $i \notin \{a-2, a-1, a\}$, $p_1^1 = p_2^2 = 1$, and $p_2^1 = -1$. The matrix p_i^a is hence a $n_T \times n_T$ square matrix, where n_T is the number of tomographic bins, with non-zero elements only in a diagonal band of a width of 3:

$$\begin{bmatrix} 1.0 & 0.0 & 0.0 & 0.0 & 0.0 & 0.0 \\ -1.0 & 1.0 & 0.0 & 0.0 & 0.0 & 0.0 \\ 0.231 & -1.231 & 1.0 & 0.0 & 0.0 & 0.0 \\ 0.0 & 1.052 & -2.053 & 1.0 & 0.0 & 0.0 \\ 0.0 & 0.0 & 0.305 & -1.304 & 1.0 & 0.0 \\ 0.0 & 0.0 & 0.0 & 0.717 & -1.717 & 1.0 \end{bmatrix}, \quad (16)$$

as the example BNT matrix. This example BNT matrix is calculated using the KiDS redshift distribution shown

in Figure 1 and the so-called ‘True Background Cosmology’ (TBC) used in our previous works [42, 45].

Same as the Gu *et al.* [42], we apply the BNT transform to the data vector:

$$\hat{C}^{a,b}(\ell) = p_i^a p_j^b C_\ell^{i,j} \quad (17)$$

and apply ℓ -cut based on this new data vector.

III. DATA AND LIKELIHOOD

A. KiDS-Legacy

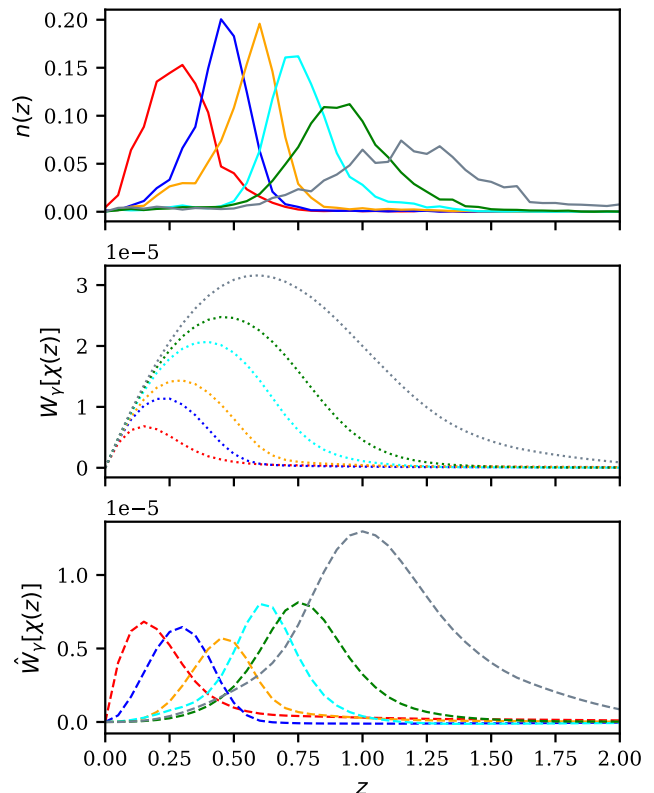


FIG. 1. Panel 1 of 3: The redshift distribution of the KiDS-Legacy Survey. Panel 2 of 3: The lensing kernel of the corresponding redshift distribution of Panel 1. Panel 3 of 3: The BNT-transformed lensing kernel from Panel 2 with the transformation matrix shown in the Equation 16.

In this work, we make use of the KiDS-Legacy cosmic shear dataset, drawn from the fifth and final data release [30] of the Kilo Degree Survey (KiDS; [28]). KiDS is a wide-field photometric imaging survey carried out by the European Southern Observatory, combining observations from two facilities: the VLT Survey Telescope (VST; [53, 54]) and the Visible and Infrared Survey Telescope for Astronomy (VISTA; [55, 56]). The survey provides measurements of galaxy positions, shapes, and orientations, which form the basis of cosmic shear analyses. Relative to the previous fourth data release, KiDS-1000 [57, 58], which covered 1006 deg² before masking

(773.3 deg² after masking), the fifth data release expands the survey area to 1347 deg² before masking (967.4 deg² after masking). In addition, the photometric redshift limit of the lensing sample is extended from $z = 1.2$ to $z = 2$, while the effective source number density increases from 7.55 arcmin⁻² to 8.79 arcmin⁻². These improvements result in a 45.6% increase in the number of source galaxies.

The galaxy samples are constructed using imaging in four optical bands (u, g, r, i) from the VST with OmegaCAM [29], together with five near-infrared bands (Z, Y, J, H, K_s) from the VIKING survey (VISTA Kilo-Degree Infrared Galaxy Survey; [59]). Compared to the fourth data release, the fifth release introduces an additional set of repeated i -band observations reaching greater depth. These deeper i -band measurements are specifically designed to improve the robustness of the photometric redshift quality [30]. Beyond the wide-field photometric data, the KiDS-Legacy survey also includes the 27 deg² KiDZ dataset, which consists of observations of several identified deep spectroscopic survey fields (e.g., [60–64]), are used for improving the redshift calibration of the main survey.

In the KiDS-Legacy analysis, photometric redshifts for source galaxies are estimated using the BPZ (Bayesian Photo- z , [65]) algorithm. The photometric redshift calibration is carried out using a combination of colour-based self-organising map (SOM; [66–68]) techniques and spatial clustering methods, with the KiDZ galaxy sample providing accurate spectroscopic redshift information. The extension of the KiDS lensing sample to $z = 2$ allows the source population to be divided into a larger number of tomographic bins than was possible in the KiDS-1000 analysis. This increase in tomographic resolution is particularly important for the application of the BNT formalism, which benefits from (and in practice requires) a sufficiently large number of redshift bins. For this reason, KiDS-Legacy provides a natural and well-matched dataset for testing the BNT-based pipeline developed in [42, 45]. Accordingly, the KiDS-Legacy source galaxies are divided into six tomographic bins defined by their BPZ redshift estimates: $0.10 < z_B^1 \leq 0.42 < z_B^2 \leq 0.58 < z_B^3 \leq 0.71 < z_B^4 \leq 0.90 < z_B^5 \leq 1.14 < z_B^6 \leq 2.00$. The inferred redshift distributions, together with the corresponding lensing kernels and their BNT-transformed counterparts, are shown in Fig. 1.

The galaxy ellipticities are measured and calibrated by the *lensfit* dedicated to KiDS DR5. We direct the reader to Wright *et al.* [30] for technical details. In this work, we pixelise the ellipticity into a HEALPIX scheme [69] to measure the pseudo- C_ℓ . The ellipticity in each pixel is given as

$$e_s(p) = \frac{\sum_{i \in p} w_i e_{s,i}}{\sum_{i \in p} w_i}, \quad (18)$$

where w_i is the *lensfit* weights, $e_s(p)$ is the pixel value of component s in the p -th pixel. $\sum_{i \in p}$ means sum-

ming up quantities of galaxies that fall in the p -th pixel. Before pixelisation, the multiplicative and additive bias have been corrected in the ellipticities.

Weight maps are required to measure the pseudo- C_ℓ . Here we use the ‘‘SW’’ weight map given in Nicola *et al.* [70]:

$$w(p) = \sum_{i \in p} w_i. \quad (19)$$

B. Pseudo- C_ℓ

In this work, we use the pseudo- C_ℓ method [47] to practically estimate the angular power spectra. This approach effectively quantifies 2-point functions in harmonic space, offering a direct connection to theoretical predictions. Additionally, it adeptly accounts for the ‘mode coupling’ arising from the footprint mask and addresses anisotropic weighting (such as footprint, lensing weight, and partially covered pixels) factors within the footprint.

Pseudo- C_ℓ can be applied to correlations between spin-0 (such as galaxy number density) and spin-2 (such as galaxy shapes) fields. In this study, we only consider cosmic shear, so we only present the pseudo- C_ℓ formalism for spin-2 \times spin-2. Assume that the sky maps of two fields u and v , with corresponding spins s_u and s_v , are the products of the underlying whole-sky fields and their respective weights, represented as $w^u(\hat{n})$ and $w^v(\hat{n})$, where \hat{n} signifies a unit vector specifying the angular position. Specifically, for binary masks that delineate only the footprint shape, $w^u(\hat{n})$ equals 1 within the footprint and 0 elsewhere. Throughout the subsequent derivations, we use a ‘tilde’ ($\tilde{}$) notation to signify quantities associated with the weighted sky.

The coupled C_ℓ is measured as:

$$\tilde{C}_\ell^{uv} = \frac{1}{2\ell + 1} \sum_m \tilde{\mathbf{a}}_{\ell m}^u \tilde{\mathbf{a}}_{\ell m}^{v\dagger}, \quad (20)$$

where $\tilde{\mathbf{a}}_{\ell m}^u$ is the harmonic coefficient of field u on weighted sky and $\tilde{\mathbf{a}}_{\ell m}^{u\dagger}$ is its complex conjugate. We use the bold symbol $\mathbf{a}_{\ell m}$ to indicate that a spin-2 field has two components, namely the E - and B -modes. The bold symbol $\tilde{\mathbf{C}}_\ell$ indicates the multiple components of pseudo- C_ℓ ’s. In the following derivation, we use the following order $\mathbf{C}_\ell = (C_\ell^{EE}, C_\ell^{EB}, C_\ell^{BE}, C_\ell^{BB})$

The coupled C_ℓ is linked to the underlying power spectra C_ℓ via

$$\tilde{\mathbf{C}}_\ell^{uv} = \sum_{\ell'} M_{\ell\ell'}(w_u, w_v) \mathbf{C}_\ell^{uv}, \quad (21)$$

where $M_{\ell\ell'}(w_u, w_v)$ is the mode-mixing matrix determined by the weight maps and spins of the two

fields. Given the angular power spectrum of the cross-correlation between the weight maps $P_\ell \equiv \sum_{m=-\ell}^{\ell} w_{\ell m}^u w_{\ell m}^{v*}$, where $w_{\ell m}^u$ is the harmonic coefficient of the weight map corresponding to field u , the forms of the mode-coupling matrix for cosmic shear is given by:

$$M_{\ell\ell'}^{22} = \begin{pmatrix} M_{\ell\ell'}^+ & 0 & 0 & M_{\ell\ell'}^- \\ 0 & M_{\ell\ell'}^- & -M_{\ell\ell'}^- & 0 \\ 0 & M_{\ell\ell'}^- & M_{\ell\ell'}^- & 0 \\ M_{\ell\ell'}^- & 0 & 0 & M_{\ell\ell'}^+ \end{pmatrix}, \text{ where} \quad (22)$$

$$M_{\ell\ell'}^\pm = \delta_{\ell\ell'} \left(\frac{2\ell' + 1}{4\pi} \right) \times \sum_{\ell''} P_{\ell''}^{uv} \begin{pmatrix} \ell' & \ell' & \ell'' \\ 2 & -2 & 0 \end{pmatrix}^2 \frac{1 \pm (-1)^{\ell+\ell'+\ell''}}{2}.$$

In the formula above, we omit the field indices in the M matrices. The expression should be understood as block matrices that are applied on $(C_{\ell m}^{EE}, C_{\ell m}^{EB}, C_{\ell m}^{BE}, C_{\ell m}^{BB})$, respectively. In addition, $\delta_{\ell\ell'}$ is the Kronecker delta symbol, and the terms in the brackets with 2 rows and 3 columns are the 3 - j symbol. Note that only ℓ'' and m are summed over, the other repeated subscripts ℓ and ℓ' are free matrix indices and are not summed over.

The true underlying power spectra can be calculated by multiplying the coupled \tilde{C}_ℓ by the inverse mode coupling matrix. In practice, it is more usual to bin the coupled pseudo- C_ℓ into bandpowers³, which will reduce the number of data points without losing information. A bandpower is the weighted C_ℓ within a range (an ℓ -bin) of ℓ . If we use q to denote the ℓ -bin index, \tilde{w}_q^ℓ as the weights at each ℓ -mode in the bin, and $\vec{\ell}_q$ as the set of ℓ 's in the q -th bin, the bandpower of coupled pseudo- C_ℓ in the q -th bin is defined as:

$$\begin{aligned} \tilde{\mathbf{C}}_q &= \sum_{\ell \in \vec{\ell}_q} \tilde{w}_q^\ell \tilde{C}_\ell \\ &= \sum_{\ell \in \vec{\ell}_q} \sum_{\ell'} \tilde{w}_q^\ell M_{\ell\ell'} C_{\ell'}. \end{aligned} \quad (23)$$

Here we omit the field and spin indices.

To obtain a good estimation of bandpower of the underlying angular power spectra, we introduce the mode-mixing matrix of bandpower by restricting ℓ' in the q' -th ℓ -bin:

$$\mathbf{M}_{qq'} \equiv \sum_{\ell \in \vec{\ell}_q} \sum_{\ell' \in \vec{\ell}_{q'}} \tilde{w}_q^\ell M_{\ell\ell'}. \quad (24)$$

Then the bandpower of coupled pseudo- C_ℓ can be formally written as

$$\tilde{\mathbf{C}}_q = \sum_{q'} \mathbf{M}_{qq'} \mathbf{C}_{q'}, \quad (25)$$

where $\mathbf{C}_{q'}$ is the bandpower of the true ℓ , which can be recovered with the inverse matrix of $\mathbf{M}_{qq'}$:

$$\mathbf{C}_q = \sum_{q'} (\mathbf{M})_{qq'}^{-1} \tilde{\mathbf{C}}_{q'}. \quad (26)$$

It should be noted that \mathbf{C}_q is not simply the true \mathbf{C}_ℓ binned with \tilde{w}_q^ℓ . Comparing Eq. 26 with Eq. 23, one can connect the bandpower with the un-binned true \mathbf{C}_ℓ :

$$\mathbf{C}_q = \sum_{\ell} w_q^\ell \mathbf{C}_\ell = \sum_{q'} (\mathbf{M})_{qq'}^{-1} \sum_{\ell \in \vec{\ell}_q} \sum_{\ell'} \tilde{w}_q^\ell M_{\ell\ell'} \mathbf{C}_{\ell'}^{uv}, \quad (27)$$

where $w_q^\ell \equiv \sum_{q'} (\mathbf{M})_{qq'}^{-1} \sum_{\ell' \in \vec{\ell}_{q'}} \tilde{w}_{q'}^{\ell'} M_{\ell\ell'}$ is the bandpower window function for the true \mathbf{C}_ℓ^{uv} . In practice, we cannot recover \mathbf{C}_ℓ^{uv} from \mathbf{C}_q^{uv} since w_q^ℓ is generally non-invertible. Instead, we compare the measured \mathbf{C}_q^{uv} with the bandpower of the theoretical \mathbf{C}_ℓ^{uv} by binning the theoretical \mathbf{C}_ℓ^{uv} with the bandpower window function w_q^ℓ .

In summary, the bandpower of pseudo- C_ℓ is measured with the following steps:

1. directly measure the coupled power spectra $\tilde{\mathbf{C}}_\ell^{uv}$ with Eq. (20);
2. calculate the mode-mixing matrix $M_{\ell\ell'}$ with Eq. (22)
3. bin the mode-mixing matrix with the given binning weight \tilde{w}_q^ℓ and get $\mathbf{M}_{qq'}$ with Eq. (24);
4. decouple the bandpower with Eq. (26) and get the bandpower \mathbf{C}_q^{uv} for the true power spectra.
5. obtain the binning weight for real angular power spectra with Eq. (27) for the following theoretical fitting.

Another consideration pertains to the smoothing effect introduced by the instrumental beam and the pixelisation window function. Assuming the smoothing is isotropic, it can be characterised by a window function denoted as b_ℓ in the harmonic space. The overall window function, encompassing all the smoothing effects, results from the multiplication of the individual window functions associated with each smoothing process. Consequently, the measured pseudo- C_ℓ becomes $\tilde{C}_\ell^{uv} \rightarrow b_\ell^u b_\ell^v \tilde{C}_\ell^{uv}$, where b_ℓ^u represents the overall window function for the field u . The PSF size of KiDS DR5 is approximately 1 arcsecond, significantly smaller than the HEALPIX pixel size employed in our analysis (1.7 arcminutes corresponding to $N_{\text{side}}=2048$). Therefore, we will ignore the smoothing effect of the instrumental beam here.

³ Note that the bandpower here refers to binned pseudo- C_ℓ , in accordance with Alonso *et al.* [47]. It is not the bandpower used in Wright *et al.* [33].

The auto-correlation pseudo- C_ℓ measured following the method above contains auto-correlated noise, namely the shape noise for cosmic shear. For angular power spectra, both are constant with shape noise equal to the shape variance σ_e^2 divided by galaxy angular number density. For pseudo- C_ℓ , we need to calculate the ‘‘mode-coupled’’ noise terms, then decouple them.

The coupled shape noise is given by Nicola *et al.* [70]:

$$\tilde{N}_\ell = \Omega_{\text{pix}} \left\langle \sum_{i \in \mathcal{P}} w_i^2 \sigma_{e,i}^2 \right\rangle_{\text{pix}}, \quad (28)$$

where Ω_{pix} is the angular area of a pixel (in steradian); $\sigma_{e,i}^2 \equiv (e_1^2 + e_2^2)/2$ is the variance of galaxy ellipticities; and $\langle \cdot \rangle_{\text{pix}}$ is the average of pixel values across the whole map. After getting the coupled noise terms, they are decoupled following the same procedure described above, then subtracted from the pseudo- C_ℓ .

For a more comprehensive theoretical treatment of pseudo- C_ℓ measurements, we direct the reader to [47]. The implementation of pseudo- C_ℓ measurements is available in the publicly-accessible **NaMaster** package⁴, which will be employed in this study. To maintain consistency with existing literature, throughout the remainder of this paper, we continue to use C_ℓ to denote binned angular power spectra. Here, ℓ should be understood as the ‘‘effective ℓ -mode’’ corresponding to each bin. In this work, the BNT transformation will be applied to pseudo- C_ℓ measured from the KiDS-Legacy data.

C. Scale Cuts

We adopt the methodology introduced in Paper I [42] and further developed in Paper II [45], which provides a framework to identify the ℓ -range $\ell_{\text{low}} < \ell < \ell_{\text{high}}$ corresponding to a given physical k -band interval $k_{\text{low}} < k < k_{\text{high}}$ for a specified level of accuracy. Within this ℓ -interval, the resulting data vector remains accurate to the desired precision. The mapping between k -space and ℓ -space cuts, for both BNT-transformed and conventional (noBNT) data vectors, is quantified using the dimensionless ratios $\hat{\mathfrak{R}}$:

$$\begin{aligned} \hat{\mathfrak{R}}^{(a,b)}(\ell; k_{\text{cuts}}, \Pi^0) &\equiv \frac{\hat{C}_{[k_{\text{low}}, k_{\text{high}}]}^{a,b}(\ell; \Pi^0)}{\hat{C}_{[k_{\text{min}}, k_{\text{max}}]}^{a,b}(\ell; \Pi^0)} \\ \mathfrak{R}^{(i,j)}(\ell; k_{\text{cuts}}, \Pi^0) &\equiv \frac{C_{[k_{\text{low}}, k_{\text{high}}]}^{i,j}(\ell; \Pi^0)}{C_{[k_{\text{min}}, k_{\text{max}}]}^{i,j}(\ell; \Pi^0)}, \end{aligned} \quad (29)$$

where $k_{\text{min}} = 0.0025 \text{ Mpc}^{-1}$ and $k_{\text{max}} = 100 \text{ Mpc}^{-1}$ define the full computational domain in k -space. The

$\hat{\mathfrak{R}}$ ratios quantify the fraction of angular power that remains after applying a k -band cut at each ℓ , comparing the k -limited spectrum (numerator) to the full-spectrum case (denominator). As emphasised in Paper I, the BNT transform does not require the use of the true cosmological parameters.

To translate a k -band cut into the corresponding ℓ -range, we introduce a tolerance region defined by $\mathfrak{R} = 1 \pm \mathcal{T}_{\text{FD}}$, where \mathcal{T}_{FD} sets the allowed fractional deviation. This parameter can be chosen by the user according to the maximum bias in the angular power spectrum that is acceptable, and is generally determined by the precision required for a given cosmological parameter (e.g., S_8) to discriminate between different cosmological models or independent measurements (such as Planck versus weak lensing constraints on S_8). In our implementation, a single value of \mathcal{T}_{FD} is applied uniformly to all elements of the data vector. To account for the effects of both k_{cuts} and \mathcal{T}_{FD} , we employ the continuous Boolean weight function $\mathcal{V}(\ell; k_{\text{cuts}}, \mathcal{T}_{\text{FD}})$:

$$\mathcal{V}(\ell; k_{\text{cuts}}, \mathcal{T}_{\text{FD}}) = \begin{cases} 1, & |\mathfrak{R}(\ell; k_{\text{cuts}}, \Pi^0) - 1| \leq \mathcal{T}_{\text{FD}} \\ 0, & |\mathfrak{R}(\ell; k_{\text{cuts}}, \Pi^0) - 1| > \mathcal{T}_{\text{FD}}, \end{cases} \quad (30)$$

where $\mathfrak{R}(\ell; k_{\text{cuts}}, \Pi^0)$ represents the dimensionless ratio of the angular power spectra computed from the full tomographic data vector. This definition applies equally to both the BNT-transformed and conventional (noBNT) data vectors. In the likelihood evaluation, the Boolean weight function is applied as follows:

$$\begin{aligned} \Delta \mathcal{D}^* &\equiv \mathcal{V}(\ell; k_{\text{cuts}}, \mathcal{T}_{\text{FD}}) (\mathcal{C}(\Pi) - \mathcal{C}(\Pi^0)) \\ \mathbb{C}^* &\equiv \mathcal{V}(\ell; k_{\text{cuts}}, \mathcal{T}_{\text{FD}}) \cdot \mathbb{C} \cdot \mathcal{V}(\ell; k_{\text{cuts}}, \mathcal{T}_{\text{FD}})^T \\ \chi^2(\Pi; k_{\text{cuts}}, \mathcal{T}_{\text{FD}}) &= \Delta \mathcal{D}^{*T} \cdot (\mathbb{C}^*)^{-1} \cdot \Delta \mathcal{D}^*, \end{aligned} \quad (31)$$

where $\mathcal{C}(\Pi)$ denotes the full tomographic data vector. Its structure follows a systematic ordering of all tomographic cross- and auto-power spectra:

$$\mathcal{C}_{[k_1, k_2]}(\Pi) = \begin{pmatrix} [\tilde{C}_{[k_1, k_2]}^{1,1}(\ell; \Pi)] \text{ all } \ell' s \\ [\tilde{C}_{[k_1, k_2]}^{1,2}(\ell; \Pi)] \text{ all } \ell' s \\ [\tilde{C}_{[k_1, k_2]}^{1,3}(\ell; \Pi)] \text{ all } \ell' s \\ \dots \\ [\tilde{C}_{[k_1, k_2]}^{5,6}(\ell; \Pi)] \text{ all } \ell' s \\ [\tilde{C}_{[k_1, k_2]}^{6,6}(\ell; \Pi)] \text{ all } \ell' s \end{pmatrix}. \quad (32)$$

In this construction, the \mathcal{V} weight ensures that only the ℓ -modes consistent with the chosen k -band cuts and fractional tolerance \mathcal{T}_{FD} contribute to both the residual $\Delta \mathcal{D}^*$ and the corresponding covariance matrix \mathbb{C}^* in each case. This formulation applies equally to the BNT-transformed

⁴ <https://namaster.readthedocs.io/en/latest/>

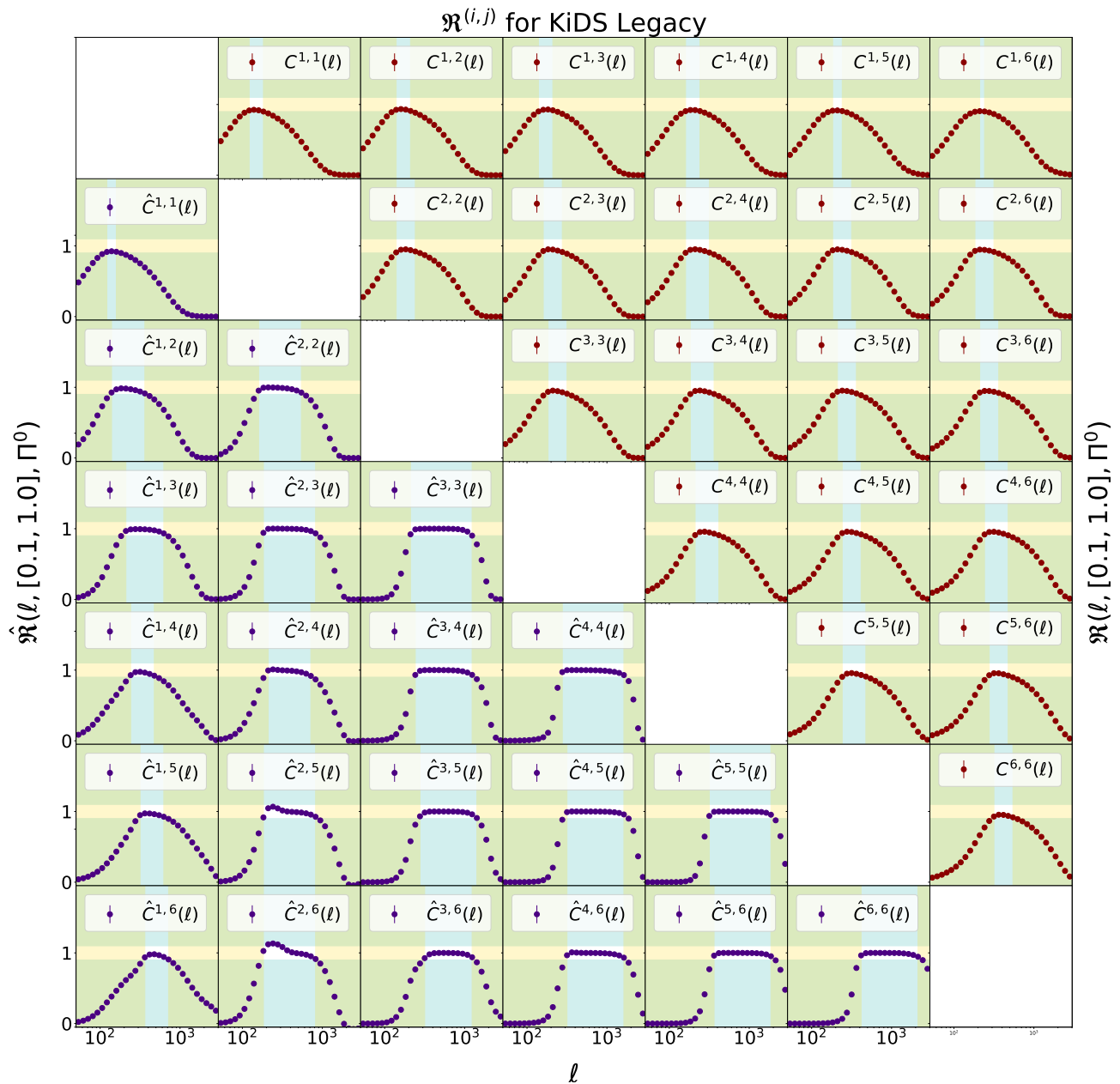


FIG. 2. Ratio of the data vector with k_{cut} to the full data vector (defined in Equation 29) for the noBNT case $\mathfrak{R}^{(i,j)}(\ell; k_{\text{cuts}}, \Pi^0)$ (upper-right triangle) and the BNT case $\hat{\mathfrak{R}}^{(a,b)}(\ell; k_{\text{cuts}}, \Pi^0)$ (lower-left triangle). Each panel shows the ratio for the combination of tomographic bins indicated by (i, j) (for the noBNT case) and (a, b) (for the BNT case). For each tomographic bin, the curves are used to define which cut in ℓ corresponds to the constraint that modes $k > k_{\text{cut}}^*$ and $k < k_{\text{cut}}^\dagger$ should not bias the data vector at a level exceeding \mathcal{T}_{FD} for $\ell_{\text{cut}}^\dagger < \ell < \ell_{\text{cut}}^*$ for noBNT (resp. $\hat{\ell}_{\text{cut}}^{(a,b)} < \ell < \hat{\ell}_{\text{cut}}^{*(a,b)}$ for BNT). All plots are given for $k_{\text{cuts}} = (0.1 \text{ Mpc}^{-1}, 1.0 \text{ Mpc}^{-1})$, and the horizontal bright band indicates the fractional threshold $\mathcal{T}_{\text{FD}} = \pm 0.1$. For each tomographic bin combination, the cut in ℓ is shown as the boundary of the cyan and green regions.

and conventional (noBNT) data vectors, maintaining the integrity of the likelihood evaluation under the k -cut scheme. The distinction between $\tilde{C}^{i,j}(\ell)$ and $\hat{C}^{a,b}(\ell)$ lies in the labeling of tomographic bins, with i, j referring to the conventional (noBNT) bins and a, b to the BNT-transformed bins. Figure 2 presents the power spectrum

ratios for both BNT and noBNT, computed under a specific k -band cut for all tomographic bin combinations in the KiDS-Legacy dataset.

D. Covariance Matrices

The covariance matrix of pseudo- C_ℓ is modelled as a summation of a Gaussian covariance, connected non-Gaussian covariance, and super-sample covariance (SSC):

$$\mathbb{C}_{pC_\ell} = \mathbb{C}_{pC_\ell}^G + \mathbb{C}_{C_\ell}^{nG} + \mathbb{C}_{C_\ell}^{SSC}. \quad (33)$$

Here, the Gaussian pseudo- C_ℓ covariance, $\mathbb{C}_{pC_\ell}^G$, is computed following the method given by García-García *et al.* [48] with narrow kernel approximation [NKA, 70]. The calculation is conducted with the NaMaster package, given the lensing weight maps. The angular power spectra C_ℓ to calculate the Gaussian covariance are obtained either from the theoretically calculated data vector using PYCCL [71] or from the observed KiDS-Legacy data vector. For posterior samples obtained using differently constructed covariance matrices, we adopt the following abbreviations: TDC denotes the theoretical-data-vector-based covariance, while ODC denotes the observational-data-vector-based covariance. In all cases, the likelihoods are evaluated using the same KiDS-Legacy observational data vector.

In this work, we only consider the leading term of the connected non-Gaussian covariance and SSC covariance from the one-halo component of the tri-spectra. Both terms are obtained from the OneCovariance package [72] with the survey geometry from standard KiDS-Legacy footprint described in Section III A and in Wright *et al.* [33]. The cosmological parameters that we use to calculate theoretical angular power spectra for the Gaussian term, as well as the tri-spectra for non-Gaussian and SSC covariances, are adopted from KiDS-Legacy cosmic shear cosmology [33].

E. Analysis setup

The analysis setup for this work combines the methodology from our Paper I [42] with the fiducial analysis of KiDS-Legacy [33]. We perform a series of Bayesian posterior estimations to quantify the impact of intrinsic alignment, using both a theoretical mock data vector based on a ‘True Background Cosmology’ (TBC) and the observational pseudo- C_ℓ data vector derived from the KiDS-Legacy shape catalogue. To recapitulate the fiducial cosmological results of the KiDS-Legacy survey, we adopt parameter priors (Please see Table I and the Figure 3 of Wright *et al.* [33] for the D^{CC} redshift error correlation matrix) almost identical to those used in the KiDS-Legacy fiducial analysis [33].

In our main analysis, we use 30 logarithmically spaced ℓ -bins, with bin centres ranging from $\ell_{\text{min}} = 50$ to $\ell_{\text{max}} = 3000$. It is worth noting that the fiducial bandpower analysis, which is different from pseudo- C_ℓ , of KiDS-Legacy used $\ell_{\text{min}} = 100$ to $\ell_{\text{max}} = 1500$. Therefore, we also use our data vector with the corresponding ℓ -cut to check our consistency with Wright *et al.* [33]. All theoretical computation in the posterior sampling process, except for the

TABLE I. The prior of all the parameters used in our sampling. $\mathcal{U}(a, b)$ is a flat prior between a and b , and $\mathcal{N}(c, d)$ is a Gaussian prior centred at c with standard deviation d . The definition of nuisance parameters below and the correlation matrix of the redshift uncertainty $\delta_{z,i}$ is given in Wright *et al.* [33].

Parameters	Fiducial Value	Priors
S_8	0.7970	$\mathcal{U}(0.5, 1.0)$
$\Omega_c h^2$	0.1530	$\mathcal{U}(0.051, 0.255)$
$\Omega_b h^2$	0.0225	$\mathcal{U}(0.019, 0.026)$
n_s	0.9690	$\mathcal{U}(0.83, 1.11)$
h	0.6898	$\mathcal{U}(0.63, 0.83)$
T_{AGN}	7.8000	$\mathcal{U}(7.3, 8.3)$
A_{IA}	0.0	$\mathcal{U}(-0.6, 0.6)$
m_1	-0.023	$\mathcal{N}(-0.023, 0.0060)$
m_2	-0.016	$\mathcal{N}(-0.016, 0.0060)$
m_3	-0.011	$\mathcal{N}(-0.011, 0.0070)$
m_4	0.0200	$\mathcal{N}(0.0200, 0.0070)$
m_5	0.0300	$\mathcal{N}(0.0300, 0.0080)$
m_6	0.0450	$\mathcal{N}(0.0450, 0.0090)$
$\delta_{z,1}$	-0.026	$\mathcal{N}(-0.026, 0.0102)$
$\delta_{z,2}$	0.0140	$\mathcal{N}(0.0140, 0.0100)$
$\delta_{z,3}$	-0.002	$\mathcal{N}(-0.002, 0.0102)$
$\delta_{z,4}$	0.0080	$\mathcal{N}(0.0080, 0.0100)$
$\delta_{z,5}$	-0.011	$\mathcal{N}(-0.011, 0.0102)$
$\delta_{z,6}$	0.0540	$\mathcal{N}(0.0540, 0.0108)$

BNT transform and pseudo- C_ℓ -related computations, is computed with the Core Cosmology Library (CCL) [71], a publicly available and standardised library for calculating cosmological observables. CCL is developed and maintained by the LSST Dark Energy Science Collaboration (DESC) [73]. We sample our parameter posteriors’ likelihood with the NAUTILUS package [74], a highly efficient importance-nested sampling toolkit designed for Bayesian posterior and evidence estimation.

IV. RESULTS

A. Consistency Check and effect on ℓ_{min}

We first verify that the cosmological constraints derived from our KiDS-Legacy pseudo- C_ℓ analysis are consistent with the fiducial KiDS-Legacy results reported in Wright *et al.* [33]. Figure 3 demonstrates that our validation posterior recovers $S_8 = 0.787_{-0.023}^{+0.031}$ for the ODC result and $S_8 = 0.795_{-0.025}^{+0.030}$ for the TDC result, in good agreement with the KiDS-Legacy bandpower result of $S_8 = 0.797_{-0.024}^{+0.023}$ for the ℓ -range $100 < \ell < 1500$, for both noBNT and BNT cases, as they are expected to be identical to each other when there is no physical scale cut applied.

We also note that, in ODC contours when the additional ℓ -ranges $50 < \ell < 100$ and $1500 < \ell < 3000$ are included in the ODC posteriors, the S_8 constraint shifts downward to $S_8 = 0.768_{-0.023}^{+0.023}$. Although this effect is not significant, it suggests a slight preference for

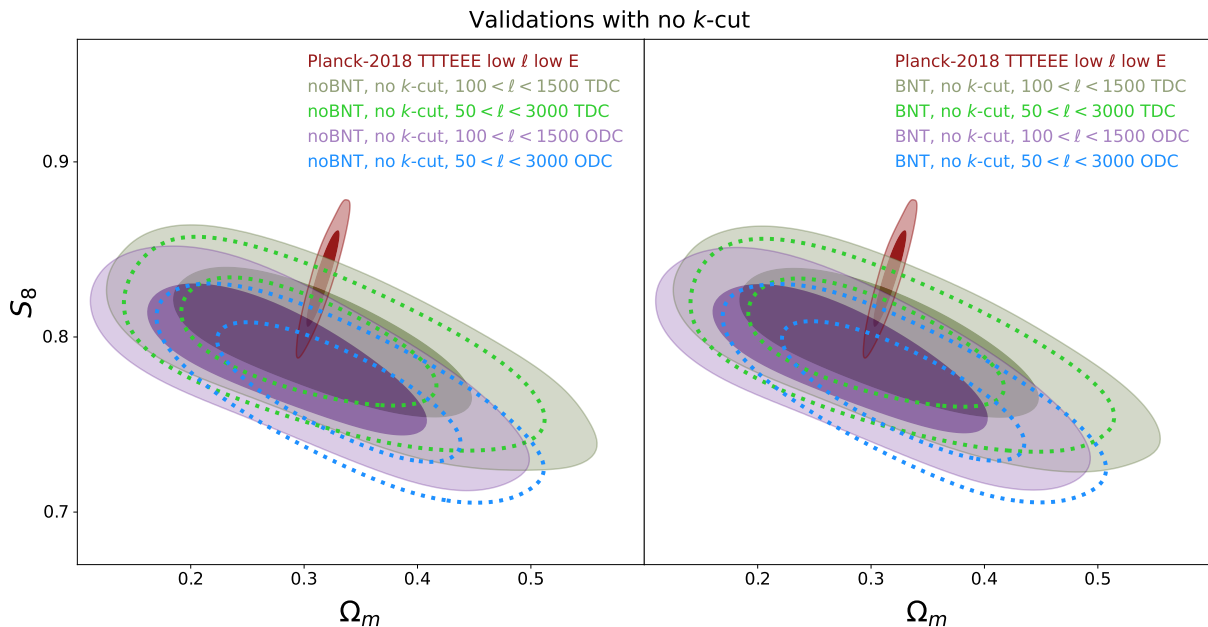


FIG. 3. Constraints in the (Ω_m, S_8) plane for the noBNT (left panel) and BNT (right panel) from the KiDS-Legacy pseudo- C_ℓ validation posteriors. For both noBNT and BNT, we show the constraint with four cases: the KiDS-Legacy like $100 < \ell < 1500$ ℓ -cut (Filled contours), and the $50 < \ell < 3000$ ℓ -cut (dotted contours), both inferred with either the theoretical data-vector-based covariance matrix (TDC) setup (blue contours) or the observational data-vector based covariance matrix (ODC) setup (green contours). The noBNT and BNT contours are expected to reproduce each other when no k -cut is applied. The red filled contour is the TTTEEE-low ℓ -lowE cosmological posterior coming from Planck Collaboration *et al.* [16].

lower S_8 values from the extended scales. This trend does not appear in the TDC posteriors. When we include the same additional ℓ -ranges, $50 < \ell < 100$ and $1500 < \ell < 3000$, the S_8 constraint remains almost unchanged, with $S_8 = 0.794^{+0.022}_{-0.022}$. This indicates that the shift in the ODC posteriors does not originate solely from the data vector, but is likely related to the covariance matrix.

B. Constraint with truncations in k -space

In Gu *et al.* [42], we showed that the exclusion of the small-scale signal through the BNT transform can effectively remove the astrophysical biases while preserving the constraining power on information of cosmological structure formation history. Using the real data, we make the same test and have the following S_8 constraint with three k_{high} values: $k < 0.1 \text{ Mpc}^{-1}$ (ODC: $S_8 = 0.664^{+0.095}_{-0.150}$; TDC: $S_8 = 0.719^{+0.131}_{-0.159}$), $k < 0.33 \text{ Mpc}^{-1}$ (ODC: $S_8 = 0.717^{+0.047}_{-0.046}$; TDC: $S_8 = 0.798^{+0.045}_{-0.045}$), and $k < 1.0 \text{ Mpc}^{-1}$ (ODC: $S_8 = 0.756^{+0.032}_{-0.032}$; TDC: $S_8 = 0.810^{+0.032}_{-0.030}$)⁵, where we show both ODC and TDC contours of $k < 0.33 \text{ Mpc}^{-1}$ in Figure 4.

⁵ Please note that the contour plots are smoothed, whereas the median and error bar values are not.

We see that constraints with different scale cuts are consistent with each other within 1.5σ , indicating that the S_8 constraint of the KiDS-Legacy dataset does not have a significant bias from the nonlinear scale. However, another interesting pattern is that the larger scales prefer a lower value of S_8 , particularly in the ODC-based posterior sampling results. For the $k < 0.33 \text{ Mpc}^{-1}$ cut, the ODC-based S_8 posterior deviates from Planck at the 2.32σ level. In contrast, the corresponding TDC-based constraint reduces the tension with Planck to 0.76σ . This suppression at the large-scale might originate from the case where the data vector fluctuates downward at large-scales, and the ODC covariance will also fluctuate downward at the large scale. Therefore, the resulting posterior will put more weight on those values than it supposed to be, and hence the posterior would prefer an even lower S_8 than in the TDC case.

In Gu *et al.* [45], we also demonstrated that comparing cosmological constraints obtained from different cuts in the k -band provides a critical diagnostic to identify potential modelling biases in the posterior sampling process. For the real data, similarly, we have the following S_8 constraint with three k_{cuts} values: $k \in (0.033, 0.33) \text{ Mpc}^{-1}$ (ODC: $S_8 = 0.749^{+0.056}_{-0.056}$; TDC: $S_8 = 0.806^{+0.051}_{-0.051}$), $k \in (0.1, 1.0) \text{ Mpc}^{-1}$ (ODC: $S_8 = 0.790^{+0.057}_{-0.049}$; TDC: $S_8 = 0.806^{+0.065}_{-0.047}$), and $k \in (0.33, 3.3) \text{ Mpc}^{-1}$ (ODC: $S_8 = 0.833^{+0.044}_{-0.044}$; TDC: $S_8 = 0.819^{+0.044}_{-0.043}$), where we show both ODC and TDC contours of $k \in (0.33, 3.3) \text{ Mpc}^{-1}$

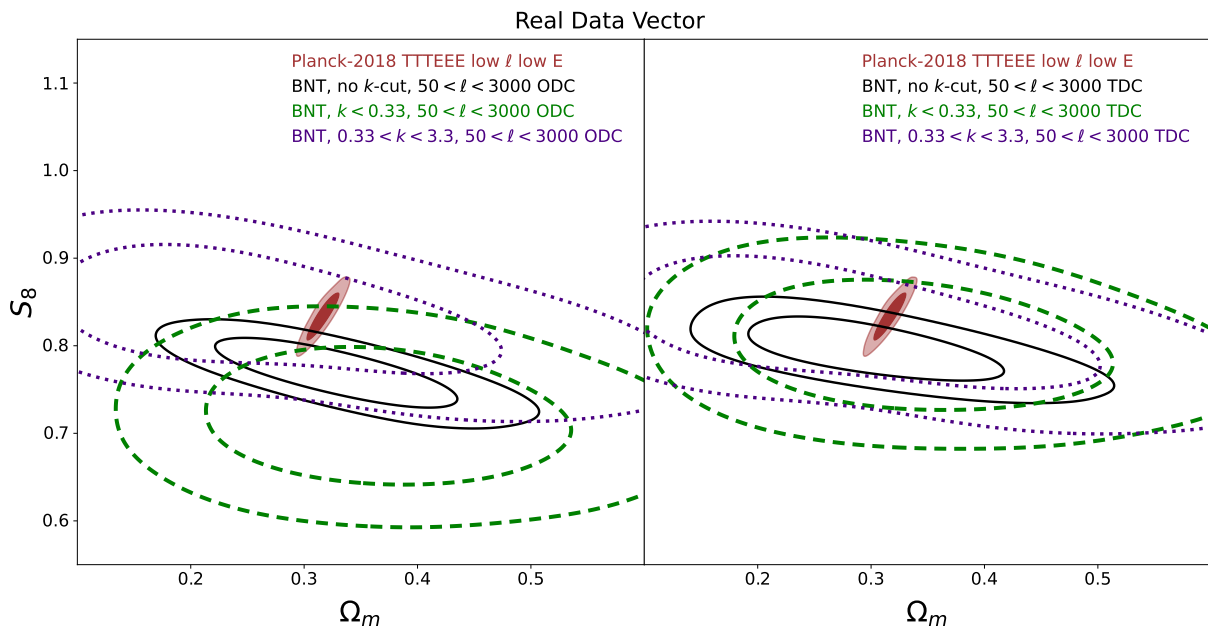


FIG. 4. Constraints in the (Ω_m, S_8) plane for the ODC-BNT (left panel) and TDC-BNT (right panel) from the **real** KiDS-Legacy pseudo- C_ℓ posteriors. We show the case without a k -cut (black solid) and two contours with different k -space scale selections: $k < 0.33 \text{ Mpc}^{-1}$ (green dashed), $k \in (0.33, 3.3) \text{ Mpc}^{-1}$ (indigo dotted). For all contours here, we use the fractional difference threshold of $\mathcal{T}_{\text{FD}} = 0.1$. The red filled contour is the TTTEEE-low ℓ -lowE cosmological posterior coming from Planck Collaboration *et al.* [16].

in Figure 4 as well, showing the largest discrepancy to the $k < 0.33 \text{ Mpc}^{-1}$ in the ODC result.

We find that, for the TDC contours, the S_8 constraints obtained from different k -bands are highly consistent with each other. This indicates that the cosmological constraints using the theoretical data-vector-based covariance matrix is self-consistent internally. However, we observe a S_8 trend in the ODC contours – a 1.24σ deviation between the constraints from the largest-scale bin, $k \in (0.033, 0.33)$, and the smallest-scale bin, $k \in (0.33, 3.3)$. While this difference is not statistically significant, it may stem from various sources. A similar, though weaker, trend, although not shown in Figures, is also present in the noBNT contours with $\mathcal{T}_{\text{FD}} = 0.1$, yielding $S_8 = 0.774 \pm 0.045$ for $k \in (0.033, 0.33)$, $S_8 = 0.811 \pm 0.036$ for $k \in (0.1, 1.0)$, and $S_8 = 0.828 \pm 0.037$ for $k \in (0.33, 3.3)$. This suggests that the observed scale-dependent trend does not originate from the BNT transformation of the data vector or the BNT transformation of the observational data-vector-based covariance matrix.

C. Cosmological Pipeline Implications

The large-scale bias in the likelihood based on the observational-data-vector covariance matrix does not appear to be a direct consequence of the covariance matrix when tested on a noiseless mock data vector. When the theoretical prediction is used as the mock data vector, the likelihoods obtained with the theoretical-data-vector co-

variance matrix and the observational-data-vector covariance matrix produce almost the same posterior results. In Figure 5, we show this likelihood test for the mock observable, using the two scale cuts $k \leq 0.33 \text{ Mpc}^{-1}$ and $k \in (0.33, 3.3) \text{ Mpc}^{-1}$. This pair exhibits the largest mutual deviation in the likelihoods based on the observational data vector with the observational-data-vector covariance matrix. Since this mock data vector does not include noise, this test should be interpreted only as a consistency check of the covariance treatment, rather than a one-to-one reproduction of the data likelihood. Nevertheless, the similarity between the ODC and TDC mock posteriors suggests that the covariance matrix alone is unlikely to be the sole origin of the large-scale deviation seen in the ODC posterior likelihoods with the KiDS-Legacy pseudo- C_ℓ data vector.

In the appendix of Gu *et al.* [42], we proposed a method to quantify the scale-dependent contribution of the data vector to each modelling parameter for a given survey specification. For KiDS-Legacy, and for all scale cuts defined by either k_{high} or k_{cuts} , we compute the corresponding scale-wise contributions relative to the total χ^2 , evaluated by perturbing A_s by a minimal amount under the fiducial KiDS-Legacy setup. This quantity should be interpreted as a normalised, scale-dependent contribution to the total χ^2 , rather than as a direct measure of Fisher information or parameter uncertainty. This procedure yields a scale-dependent distribution of the sensitivity to A_s across k -modes, which is shown in the left panel of Figure 6. We then estimate the 1σ interval of this dis-

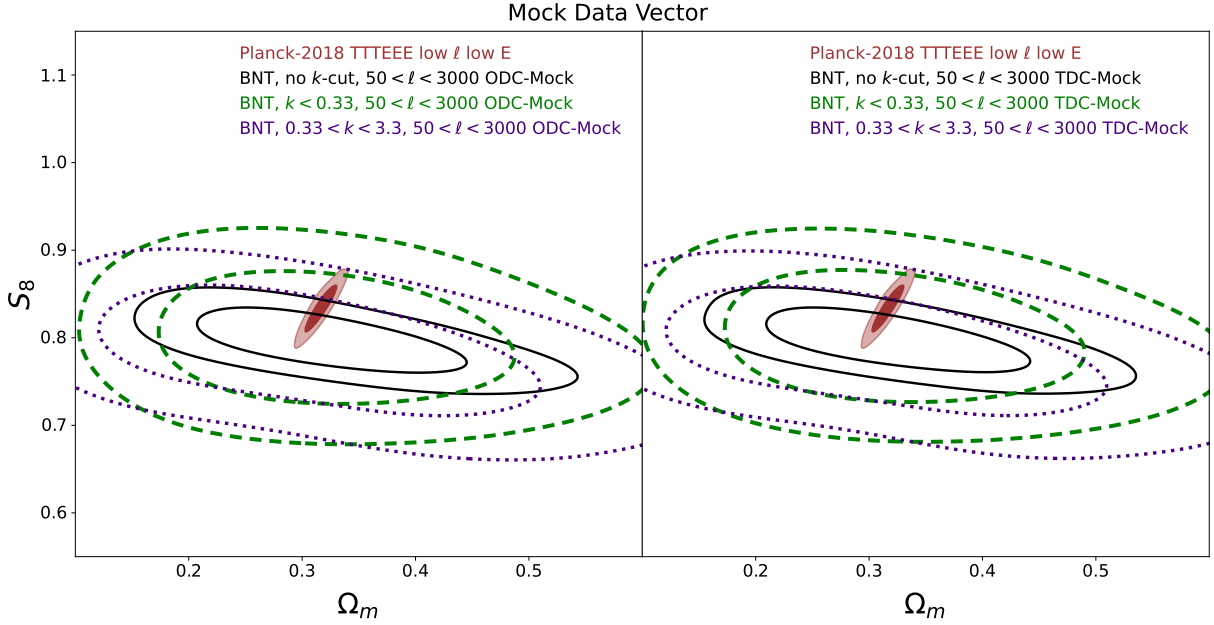


FIG. 5. Same as Fig. 4, but with **theoretical data vector** as the **mock observation** instead.

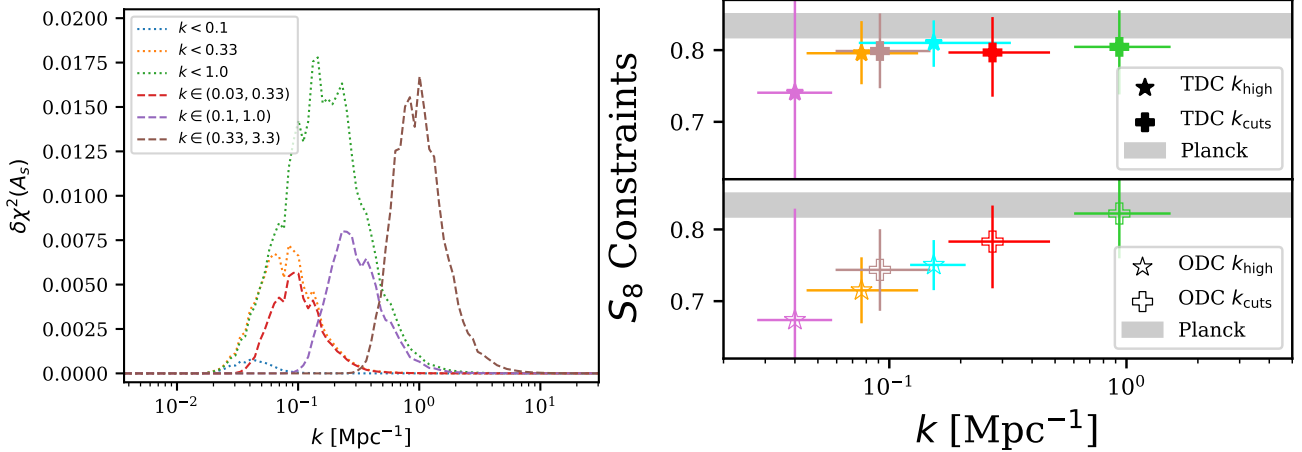


FIG. 6. Left: The contribution to the total A_s constraining power from each scale to the total χ^2 for different BNT-based k -cut choices with $\mathcal{T}_{\text{FD}} = 0.1$. Right: The constraint of S_8 of each k -cut choices with TDC (Upper half) and ODC (Lower half) setups. The S_8 errorbar of each data point comes from the weighted 16, 50, and 84% percentage of the 1-dimensional posterior on S_8 . Their errorbar on k -axis is computed from the 16, 50, and 84% percentage by treating $\delta\chi^2(k)$ as a probability distribution function. The star shape data points indicate the k_{high} truncation with only the upper limit on the k -range selection, while the cross shape data points indicate k_{cuts} truncation that have both the upper and the lower limits on the k -range selection. The grey shaded region indicates the S_8 constraint coming from the Planck TTTEEE-low ℓ -lowE result.

tribution to characterise the range of scales from which each k -cut chain receives the dominant contribution.

Using the posterior distribution of S_8 obtained from the likelihood analysis, we further present the ODC-BNT (filled markers) and TDC-BNT (empty markers) S_8 constraints associated with the k_{high} - and k_{cuts} -based scale selections in the right panel of Figure 6. We find that the TDC S_8 constraints are mostly consistent with each other, although the largest-scale cut still shows some sup-

pression. In contrast, the ODC S_8 constraints exhibit a much more obvious correlated trend in which larger physical scales, corresponding to lower k , prefer lower values of S_8 . This behaviour is consistently observed across all data points, each corresponding to a posterior analysis with a specific scale cut. The largest difference occurs between the scale ranges $k < 0.33 \text{ Mpc}^{-1}$ (orange stars) and $k \in (0.33, 3.3) \text{ Mpc}^{-1}$ (limegreen crosses), reaching a maximum deviation of 1.80σ . This level of deviation

is not statistically significant, but it remains noteworthy because such a trend is absent in the mock tests. This suggests that the large-scale preference for lower S_8 is not a generic consequence of the covariance prescription or the data vector alone. Instead, it may reflect some specific interplays between the KiDS-Legacy pseudo- C_ℓ data vector and the observational-data-vector-based Gaussian covariance matrix.

V. DISCUSSION AND CONCLUSIONS

Scale cuts in weak lensing data, whether applied in configuration space or harmonic space, are a critical component of analyses aiming to address cosmological parameter tensions, such as the S_8 discrepancy. However, because of the two-dimensional projection nature of conventional weak gravitational lensing, scale cuts are imperfect and invariably retain some contribution from unwanted scales.

The BNT transform [44] is a method that helps suppress information from these unwanted scales while preserving, as much as possible, the relevant information in both directions. Building on this approach, our previous works [42, 45] developed a methodological framework for testing theoretical modelling in the posterior sampling process and deriving cosmological constraints. In the present study, we apply this BNT-based analysis pipeline to the KiDS-Legacy cosmic shear dataset to evaluate its performance and to extract cosmological constraints across different physical scales.

We find that, across all scale cuts considered in this work, the cosmological inference remains statistically consistent. Even in the case showing the largest apparent deviation between different physical scale domains, their difference is still below 2σ . Those resulting constraints are also consistent with the fiducial KiDS-Legacy findings [33, 34], and we do not find any evidence that modelling bias or scale-dependent systematics critically affect the current KiDS-Legacy cosmic shear analysis.

Nevertheless, the BNT scale-cut analysis reveals a mild but noteworthy dependence on the covariance prescription. When the observational data vector is used both in the likelihood and in the construction of the Gaussian part of the covariance matrix (ODC), the S_8 posteriors exhibit an apparent scale-dependent trend: larger physical scales (lower k) prefer lower values of S_8 . The largest difference is found between the scale selection of $k < 0.33 \text{ Mpc}^{-1}$ and $k \in (0.33, 3.3) \text{ Mpc}^{-1}$, reaching a maximum deviation of 1.80σ . This effect is not very statistically significant, but the coherence across the scale bins makes it useful as a diagnostic of the inference pipeline.

The interpretation of this trend changes when the theoretical-data-vector (TDC) covariance matrix is used. For TDC posteriors, S_8 constraints of different scale bins are more stable across scales, and the large-scale preference for lower S_8 is reduced to 0.75σ . Mock tests using

the theoretical prediction as the mock observational data vector show almost no difference between the ODC and TDC posterior results. This indicates that the data vector alone or the covariance matrix alone either cannot generate the large-scale deviation seen in the ODC analysis of the KiDS-Legacy pseudo- C_ℓ data vector. Instead, the apparent trend appears only when the observational pseudo- C_ℓ data vector and the observational-data-vector-based Gaussian covariance matrix are used together.

This result, therefore, should not be interpreted as evidence for a departure from the standard Λ CDM model. Although the ODC posterior is counterintuitive from the perspective of many theoretical attempts to resolve the S_8 tension through late-time or small-scale modifications, the TDC posteriors, as a comparison, show that the effect is mostly sensitive to the covariance prescription used in the likelihood. Our work shows that neither the data vector nor the covariance matrix is the sole origin of the effect; the trend appears when observational data vector is used simultaneously for covariance matrix calculation and likelihood computation. This suggests that our BNT-based k -cut method provides a sensitive test of the consistency as noted in our previous paper, [45].

A possible explanation for the bias associated with the observational-data-vector covariance matrix is its treatment of the sample-variance, or cosmic-variance, contribution. If the actual observed spectrum is used in this part of the covariance calculation, the covariance matrix is no longer independent of the data vector that it is meant to weight. This introduces a data-dependent weighting of the likelihood residuals and can bias the inferred parameters, especially on large scales where cosmic variance is more important. Another possible origin of this scale-dependent sensitivity may hide in the calibration of observational ingredients entering both the data vector and the covariance matrix, including photometric redshifts, multiplicative shear bias, and noise contributions. Standard calibration methods, based on shifts and widths of the redshift distributions and effective multiplicative-bias corrections, are adequate for current Stage-III cosmic shear analyses, but the BNT k -cut method imposes more direct requirements on the accuracy of redshift-dependent information. Therefore, small inconsistencies that are subdominant in standard analyses can become more visible once the data are reorganised into physical-scale bins. In parallel, we are developing an ultrafast reconstruction method of the linear matter power spectrum based on the BNT transform. Its ultra-low computational cost makes it well suited for validating inference pipelines and for diagnosing the ODC posterior behaviour observed in this KiDS-Legacy pseudo- C_ℓ analysis.

Although the statistical significance of the S_8 tension has been reduced by recent improvements in photometric-redshift calibration [33], scale-dependent tests remain important for investigating theoretical extensions to Λ CDM and for validating the robustness of weak-lensing inference pipelines. In this work, our results

demonstrate that the BNT methodology is not only useful for isolating physical scales, but also for diagnosing theoretical-modelling systematics, data-vector characteristics, and covariance prescriptions. The main role of the BNT-based k -cut framework is not only to divide the data into different scale ranges and to mitigate nonlinear systematics, but also to provide a controlled environment in which cosmological information, observational systematics, and inference assumptions can be tested jointly.

ACKNOWLEDGMENTS

All theoretical calculations are based on PYCCL [71] and we present our whole sampling code suite in [75]. We calculate errorbars and plot posterior contours with the GETDIST [76] package. We are grateful to Gary Bernstein, Sébastien Fabbro, Sacha Guerrini, Alan Heavens, Gary Hinshaw, Mike Hudson, Martin Kilbinger, Meng-Xiang Lin, Will Percival, Levon Pogosian, and the whole German Centre for Cosmological Lensing (GCCL) for their constructive feedback during the construction of the entire structure for the study and the analysis. SG acknowledges support from the John I. Waters Research Fellowship (award No. 6701), and the Ruhr-Universität Bochum Research Scholarship for Doctoral Researchers from International Partners. SG also thanks the Herzberg Astronomy and Astrophysics Research Centre of the Canadian National Research Council for hosting him during the finalisation phase of this work. ZY is supported by JSPS KAKENHI Grant Number 23H00108 and JST FOREST Program Grant Number JPMJFR2137. LvW acknowledges support from the

Natural Sciences and Engineering Research Council of Canada (NSERC) and the Canadian Institute for Advanced Research (CIFAR). HH is supported by a DFG Heisenberg grant (Hi 1495/5-1), the DFG Collaborative Research Center SFB1491, an ERC Consolidator Grant (No. 770935), and the DLR project 50QE2305. AHW is supported by the Deutsches Zentrum für Luft- und Raumfahrt (DLR), under project 50QE2305, made possible by the Bundesministerium für Wirtschaft und Klimaschutz, and acknowledges funding from the German Science Foundation DFG, via the Collaborative Research Center SFB1491 "Cosmic Interacting Matters - From Source to Signal". MB is supported by the Polish National Science Center through grant no. 2020/38/E/ST9/00395 and by the Polish Ministry of Science and Higher Education under the agreement no. 2026/WK/06. CG is funded by the MICINN project PID2022-141079NB-C32. IFAE is partially funded by the CERCA program of the Generalitat de Catalunya. SSL has received funding from the programme "Netzwerke 2021", an initiative of the Ministry of Culture and Science of the State of Northrhine Westphalia. LL is supported by the Austrian Science Fund (FWF) [ESP 357-N] and funded in part by the Austrian Science Fund (FWF) 10.55776/F101300. LM acknowledges the financial contribution from the grant ASI n. 2024-10-HH.0 "Attività scientifiche per la missione Euclid – fase E". RR is partially supported by an ERC Consolidator Grant (No. 770935). BS acknowledges support from the Max Planck Society and the Alexander von Humboldt Foundation in the framework of the Max Planck-Humboldt Research Award endowed by the Federal Ministry of Education and Research.

-
- [1] G. R. Blumenthal, H. Pagels, and J. R. Primack, Galaxy formation by dissipationless particles heavier than neutrinos, *Nature (London)* **299**, 37 (1982).
- [2] G. R. Blumenthal, S. M. Faber, J. R. Primack, and M. J. Rees, Formation of galaxies and large-scale structure with cold dark matter., *Nature (London)* **311**, 517 (1984).
- [3] M. Davis, G. Efstathiou, C. S. Frenk, and S. D. M. White, The evolution of large-scale structure in a universe dominated by cold dark matter, *Astrophys. J.* **292**, 371 (1985).
- [4] M. Davis, J. Tonry, J. Huchra, and D. W. Latham, On the Virgo supercluster and the mean mass density of the universe., *ApJL* **238**, L113 (1980).
- [5] M. Davis and P. J. E. Peebles, A survey of galaxy redshifts. V. The two-point position and velocity correlations., *Astrophys. J.* **267**, 465 (1983).
- [6] A. H. Guth, Inflationary universe: A possible solution to the horizon and flatness problems, *Phys. Rev. D* **23**, 347 (1981).
- [7] G. F. Smoot, C. L. Bennett, A. Kogut, E. L. Wright, J. Aymon, N. W. Boggess, E. S. Cheng, G. de Amici, S. Gulkis, M. G. Hauser, G. Hinshaw, P. D. Jackson, M. Janssen, E. Kaita, T. Kelsall, P. Keegstra, C. Lineweaver, K. Loewenstein, P. Lubin, J. Mather, S. S. Meyer, S. H. Moseley, T. Murdock, L. Rokke, R. F. Silverberg, L. Tenorio, R. Weiss, and D. T. Wilkinson, Structure in the COBE Differential Microwave Radiometer First-Year Maps, *ApJL* **396**, L1 (1992).
- [8] E. L. Wright, S. S. Meyer, C. L. Bennett, N. W. Boggess, E. S. Cheng, M. G. Hauser, A. Kogut, C. Lineweaver, J. C. Mather, G. F. Smoot, R. Weiss, S. Gulkis, G. Hinshaw, M. Janssen, T. Kelsall, P. M. Lubin, S. H. Moseley, Jr., T. L. Murdock, R. A. Shafer, R. F. Silverberg, and D. T. Wilkinson, Interpretation of the Cosmic Microwave Background Radiation Anisotropy Detected by the COBE Differential Microwave Radiometer, *ApJL* **396**, L13 (1992).
- [9] A. Einstein, Kosmologische Betrachtungen zur allgemeinen Relativitätstheorie, *Sitzungsberichte der Königlich Preussischen Akademie der Wissenschaften*, 142 (1917).
- [10] M. Davis, G. Efstathiou, C. S. Frenk, and S. D. M. White, The end of cold dark matter?, *Nature (London)* **356**, 489 (1992).
- [11] N. A. Bahcall, X. Fan, and R. Cen, Constraining Ω with Cluster Evolution, *ApJL* **485**, L53 (1997), [arXiv:astro-](#)

- ph/9706018 [astro-ph].
- [12] P. J. E. Peebles and J. T. Yu, Primeval adiabatic perturbation in an expanding universe, *Astrophys. J.* **162**, 815 (1970).
- [13] D. J. Eisenstein, I. Zehavi, D. W. Hogg, R. Scoccimarro, M. R. Blanton, and et al., Detection of the baryon acoustic peak in the large-scale correlation function of sdss luminous red galaxies, *Astrophys. J.* **633**, 560 (2005).
- [14] S. Cole, W. J. Percival, J. A. Peacock, P. Norberg, C. M. Baugh, and et al., The 2df galaxy redshift survey: power-spectrum analysis of the final dataset and cosmological implications, *Mon. Not. Roy. Astron. Soc.* **362**, 505 (2005).
- [15] R. A. Sunyaev and Y. B. Zel'dovich, The observations of relic radiation as a test of the nature of x-ray radiation from the clusters of galaxies, *Comments on Astrophysics and Space Physics* **4**, 173 (1972).
- [16] Planck Collaboration, N. Aghanim, Y. Akrami, M. Ashdown, J. Aumont, C. Baccigalupi, M. Ballardini, A. J. Banday, R. B. Barreiro, N. Bartolo, S. Basak, R. Battye, K. Benabed, J. P. Bernard, M. Bersanelli, P. Bielewicz, J. J. Bock, J. R. Bond, J. Borrill, F. R. Bouchet, F. Boulanger, M. Bucher, C. Burigana, R. C. Butler, E. Calabrese, J. F. Cardoso, J. Carron, A. Challinor, H. C. Chiang, J. Chluba, L. P. L. Colombo, C. Combet, D. Contreras, B. P. Crill, F. Cuttaia, P. de Bernardis, G. de Zotti, J. Delabrouille, J. M. Delouis, E. Di Valentino, J. M. Diego, O. Doré, M. Douspis, A. Ducout, X. Dupac, S. Dusini, G. Efstathiou, F. Elsner, T. A. Enßlin, H. K. Eriksen, Y. Fantaye, M. Farhang, J. Fergusson, R. Fernandez-Cobos, F. Finelli, F. Forastieri, M. Frailis, A. A. Fraisse, E. Franceschi, A. Frolov, S. Galeotta, S. Galli, K. Ganga, R. T. Génova-Santos, M. Gerbino, T. Ghosh, J. González-Nuevo, K. M. Górski, S. Gratton, A. Gruppuso, J. E. Gudmundsson, J. Hamann, W. Handley, F. K. Hansen, D. Herranz, S. R. Hildebrandt, E. Hivon, Z. Huang, A. H. Jaffe, W. C. Jones, A. Karakci, E. Keihänen, R. Kesitalo, K. Kiiveri, J. Kim, T. S. Kisner, L. Knox, N. Krachmalnicoff, M. Kunz, H. Kurki-Suonio, G. Lagache, J. M. Lamarre, A. Lasenby, M. Lattanzi, C. R. Lawrence, M. Le Jeune, P. Lemos, J. Lesgourgues, F. Levrier, A. Lewis, M. Liguori, P. B. Lilje, M. Lilley, V. Lindholm, M. López-Cañiego, P. M. Lubin, Y. Z. Ma, J. F. Macías-Pérez, G. Maggio, D. Maino, N. Mandolesi, A. Mangilli, A. Marcos-Caballero, M. Maris, P. G. Martin, M. Martinelli, E. Martínez-González, S. Matarrese, N. Mauri, J. D. McEwen, P. R. Meinhold, A. Melchiorri, A. Mennella, M. Migliaccio, M. Milea, S. Mitra, M. A. Miville-Deschênes, D. Molinari, L. Montier, G. Morgante, A. Moss, P. Natoli, H. U. Nørgaard-Nielsen, L. Pagano, D. Paoletti, B. Partridge, G. Patanchon, H. V. Peiris, F. Perrotta, V. Pettorino, F. Piacentini, L. Polastri, G. Polenta, J. L. Puget, J. P. Rachen, M. Reinecke, M. Remazeilles, A. Renzi, G. Rocha, C. Rosset, G. Roudier, J. A. Rubiño-Martín, B. Ruiz-Granados, L. Salvati, M. Sandri, M. Savelainen, D. Scott, E. P. S. Shellard, C. Sirignano, G. Sirri, L. D. Spencer, R. Sunyaev, A. S. Suur-Uski, J. A. Tauber, D. Tavagnacco, M. Tenti, L. Toffolatti, M. Tomasi, T. Trombetti, L. Valenziano, J. Valiviita, B. Van Tent, L. Vibert, P. Vielva, F. Villa, N. Vittorio, B. D. Wandelt, I. K. Wehus, M. White, S. D. M. White, A. Zaccchi, and A. Zonca, Planck 2018 results. VI. Cosmological parameters, *Astronomy & Astrophysics* **641**, A6 (2020), arXiv:1807.06209 [astro-ph.CO].
- [17] M. Raveri and W. Hu, Concordance and discordance in cosmology, *Phys. Rev. D* **99**, 043506 (2019), arXiv:1806.04649 [astro-ph.CO].
- [18] L. Verde, T. Treu, and A. G. Riess, Tensions between the early and the late universe, *Nature Astronomy* **3**, 891 (2019), 1907.10625.
- [19] A. G. Riess, L. M. Macri, S. L. Hoffmann, D. Scolnic, S. Casertano, A. V. Filippenko, B. E. Tucker, M. J. Reid, D. O. Jones, J. M. Silverman, R. Chornock, P. Challis, W. Yuan, P. J. Brown, and R. J. Foley, A 2.4% Determination of the Local Value of the Hubble Constant, *Astrophys. J.* **826**, 56 (2016), arXiv:1604.01424 [astro-ph.CO].
- [20] C. Heymans, T. Tröster, M. Asgari, C. Blake, H. Hildebrandt, B. Joachimi, K. Kuijken, C.-A. Lin, A. G. Sánchez, J. L. van den Busch, A. H. Wright, A. Amon, M. Bilicki, J. de Jong, M. Crocce, A. Dvornik, T. Erben, M. C. Fortuna, F. Getman, B. Giblin, K. Glazebrook, H. Hoekstra, S. Joudaki, A. Kannawadi, F. Köhlinger, C. Lidman, L. Miller, N. R. Napolitano, D. Parkinson, P. Schneider, H. Shan, E. A. Valentijn, G. Verdoes Kleijn, and C. Wolf, KiDS-1000 Cosmology: Multi-probe weak gravitational lensing and spectroscopic galaxy clustering constraints, *Astronomy & Astrophysics* **646**, A140 (2021), arXiv:2007.15632 [astro-ph.CO].
- [21] L. Van Waerbeke, Y. Mellier, T. Erben, J. C. Cuillandre, F. Bernardeau, R. Maoli, E. Bertin, H. J. McCracken, O. Le Fèvre, B. Fort, M. Dantel-Fort, B. Jain, and P. Schneider, Detection of correlated galaxy ellipticities from CFHT data: first evidence for gravitational lensing by large-scale structures, *Astronomy & Astrophysics* **358**, 30 (2000), arXiv:astro-ph/0002500 [astro-ph].
- [22] N. Kaiser, G. Wilson, and G. A. Luppino, Large-Scale Cosmic Shear Measurements, *arXiv e-prints*, astro-ph/0003338 (2000), arXiv:astro-ph/0003338 [astro-ph].
- [23] D. J. Bacon, A. R. Refregier, and R. S. Ellis, Detection of weak gravitational lensing by large-scale structure, *MNRAS* **318**, 625 (2000), arXiv:astro-ph/0003008 [astro-ph].
- [24] D. M. Wittman, J. A. Tyson, D. Kirkman, I. Dell'Antonio, and G. Bernstein, Detection of weak gravitational lensing distortions of distant galaxies by cosmic dark matter at large scales, *Nature (London)* **405**, 143 (2000), arXiv:astro-ph/0003014 [astro-ph].
- [25] R. D. Blandford, A. B. Saust, T. G. Brainerd, and J. V. Villumsen, The distortion of distant galaxy images by large-scale structure., *MNRAS* **251**, 600 (1991).
- [26] N. Kaiser, Weak Gravitational Lensing of Distant Galaxies, *Astrophys. J.* **388**, 272 (1992).
- [27] M. Bartelmann and P. Schneider, Weak gravitational lensing, *Physics Reports* **340**, 291 (2001), arXiv:astro-ph/9912508 [astro-ph].
- [28] J. T. A. de Jong, G. A. Verdoes Kleijn, K. H. Kuijken, and E. A. Valentijn, The Kilo-Degree Survey, *Experimental Astronomy* **35**, 25 (2013), arXiv:1206.1254 [astro-ph.CO].
- [29] K. Kuijken, OmegaCAM: ESO's Newest Imager, *The Messenger* **146**, 8 (2011).
- [30] A. H. Wright, K. Kuijken, H. Hildebrandt, M. Radovich, M. Bilicki, A. Dvornik, F. Getman, C. Heymans, H. Hoekstra, S.-S. Li, L. Miller, N. R. Napolitano, Q. Xia, M. Asgari, M. Brescia, H. Buddelmeijer, P. Burger, G. Castignani, S. Cavuoti, J. de Jong, A. Edge, B. Giblin, C. Giocoli, J. Harnois-Déraps, P. Jalan, B. Joachimi,

- A. John William, S. Joudaki, A. Kannawadi, G. Kaur, F. La Barbera, L. Linke, C. Mahony, M. Maturi, L. Moscardini, S. J. Nakoneczny, M. Paolillo, L. Porth, E. Puddu, R. Reischke, P. Schneider, M. Sereno, H. Shan, C. Sifón, B. Stölzner, T. Tröster, E. Valentijn, J. L. van den Busch, G. Verdoes Kleijn, A. Wittje, Z. Yan, J. Yao, M. Yoon, and Y.-H. Zhang, The fifth data release of the Kilo Degree Survey: Multi-epoch optical/NIR imaging covering wide and legacy-calibration fields, *Astronomy & Astrophysics* **686**, A170 (2024), [arXiv:2503.19439 \[astro-ph.GA\]](#).
- [31] L. Miller, T. D. Kitching, C. Heymans, A. F. Heavens, and L. van Waerbeke, Bayesian galaxy shape measurement for weak lensing surveys - I. Methodology and a fast-fitting algorithm, *MNRAS* **382**, 315 (2007), [arXiv:0708.2340 \[astro-ph\]](#).
- [32] M. Asgari, C.-A. Lin, B. Joachimi, B. Giblin, C. Heymans, H. Hildebrandt, A. Kannawadi, B. Stölzner, T. Tröster, J. L. van den Busch, A. H. Wright, M. Bilicki, C. Blake, J. de Jong, A. Dvornik, T. Erben, F. Getman, H. Hoekstra, F. Köhlinger, K. Kuijken, L. Miller, M. Radovich, P. Schneider, H. Shan, and E. Valentijn, KiDS-1000 cosmology: Cosmic shear constraints and comparison between two point statistics, *Astronomy & Astrophysics* **645**, A104 (2021), [arXiv:2007.15633 \[astro-ph.CO\]](#).
- [33] A. H. Wright, B. Stölzner, M. Asgari, M. Bilicki, B. Giblin, C. Heymans, H. Hildebrandt, H. Hoekstra, B. Joachimi, K. Kuijken, S.-S. Li, R. Reischke, M. von Wietersheim-Kramsta, M. Yoon, P. Burger, N. E. Chisari, J. de Jong, A. Dvornik, C. Georgiou, J. Harnois-Déraps, P. Janan, A. J. William, S. Joudaki, G. F. Lesci, L. Linke, A. Loureiro, C. Mahony, M. Maturi, L. Miller, L. Moscardini, N. R. Napolitano, L. Porth, M. Radovich, P. Schneider, T. Tröster, A. Wittje, Z. Yan, and Y.-H. Zhang, KiDS-Legacy: Cosmological constraints from cosmic shear with the complete Kilo-Degree Survey, [arXiv e-prints](#), [arXiv:2503.19441 \(2025\)](#), [arXiv:2503.19441 \[astro-ph.CO\]](#).
- [34] B. Stölzner, A. H. Wright, M. Asgari, C. Heymans, H. Hildebrandt, H. Hoekstra, B. Joachimi, K. Kuijken, S.-S. Li, C. Mahony, R. Reischke, M. Yoon, M. Bilicki, P. Burger, N. E. Chisari, A. Dvornik, C. Georgiou, B. Giblin, J. Harnois-Déraps, P. Janan, A. J. William, S. Joudaki, G. F. Lesci, L. Linke, A. Loureiro, M. Maturi, L. Moscardini, N. R. Napolitano, L. Porth, M. Radovich, T. Tröster, E. Valentijn, M. von Wietersheim-Kramsta, A. Wittje, Z. Yan, and Y.-H. Zhang, KiDS-Legacy: Consistency of cosmic shear measurements and joint cosmological constraints with external probes, *Astronomy & Astrophysics* **702**, A169 (2025), [arXiv:2503.19442 \[astro-ph.CO\]](#).
- [35] A. Amon and G. Efstathiou, A non-linear solution to the S_8 tension?, *MNRAS* **516**, 5355 (2022), [arXiv:2206.11794 \[astro-ph.CO\]](#).
- [36] J. M. Bardeen, J. R. Bond, N. Kaiser, and A. S. Szalay, The Statistics of Peaks of Gaussian Random Fields, *Astrophys. J.* **304**, 15 (1986).
- [37] S. Gu, M.-A. Dor, L. van Waerbeke, M. Asgari, A. Mead, T. Tröster, and Z. Yan, On constraining cosmology and the halo mass function with weak gravitational lensing, *MNRAS* **525**, 4871 (2023), [arXiv:2302.00780 \[astro-ph.CO\]](#).
- [38] C. Preston, A. Amon, and G. Efstathiou, A non-linear solution to the S_8 tension - II. Analysis of DES Year 3 cosmic shear, *MNRAS* **525**, 5554 (2023), [arXiv:2305.09827 \[astro-ph.CO\]](#).
- [39] M. White, R. Zhou, J. DeRose, S. Ferraro, S.-F. Chen, N. Kokron, S. Bailey, D. Brooks, J. García-Bellido, J. Guy, K. Honscheid, R. Kehoe, A. Kremin, M. Levi, N. Palanque-Desabrouille, C. Poppett, D. Schlegel, and G. Tarle, Cosmological constraints from the tomographic cross-correlation of DESI Luminous Red Galaxies and Planck CMB lensing, *JCAP* **2022**, 007 (2022), [arXiv:2111.09898 \[astro-ph.CO\]](#).
- [40] M.-X. Lin, B. Jain, M. Raveri, E. J. Baxter, C. Chang, M. Gatti, S. Lee, and J. Muir, Late time modification of structure growth and the S_8 tension, *Phys. Rev. D* **109**, 063523 (2024), [arXiv:2308.16183 \[astro-ph.CO\]](#).
- [41] K. Naidoo, M. Jaber, W. A. Hellwing, and M. Bilicki, Dark matter solution to the H_0 and S_8 tensions, and the integrated Sachs-Wolfe void anomaly, *Phys. Rev. D* **109**, 083511 (2024), [arXiv:2209.08102 \[astro-ph.CO\]](#).
- [42] S. Gu, L. van Waerbeke, F. Bernardeau, and R. Dalal, Mitigating nonlinear systematics in weak lensing surveys: The Bernardeau-Nishimichi-Taruya approach, *Phys. Rev. D* **111**, 083530 (2025), [arXiv:2412.14704 \[astro-ph.CO\]](#).
- [43] M. P. van Daalen, I. G. McCarthy, and J. Schaye, Exploring the effects of galaxy formation on matter clustering through a library of simulation power spectra, *MNRAS* **491**, 2424 (2020), [arXiv:1906.00968 \[astro-ph.CO\]](#).
- [44] F. Bernardeau, T. Nishimichi, and A. Taruya, Cosmic shear full nulling: sorting out dynamics, geometry and systematics, *MNRAS* **445**, 1526 (2014), [arXiv:1312.0430 \[astro-ph.CO\]](#).
- [45] S. Gu, L. van Waerbeke, F. Bernardeau, and S. Fabbro, Mitigating nonlinear systematics in weak lensing surveys II: Stability and Diagnostics under Intrinsic Alignment, *Phys. Rev. D* **113**, 023528 (2026), [arXiv:2511.09544 \[astro-ph.CO\]](#).
- [46] P. L. Taylor, F. Bernardeau, and E. Huff, x-cut Cosmic shear: Optimally removing sensitivity to baryonic and nonlinear physics with an application to the Dark Energy Survey year 1 shear data, *Phys. Rev. D* **103**, 043531 (2021), [arXiv:2007.00675 \[astro-ph.CO\]](#).
- [47] D. Alonso, J. C. Hill, R. Hložek, and D. N. Spergel, Measurement of the thermal sunyaev-zel'dovich effect around cosmic voids, *Phys. Rev. D* **97**, 10.1103/physrevd.97.063514 (2018).
- [48] C. García-García, D. Alonso, and E. Bellini, Disconnected pseudo-cl covariances for projected large-scale structure data, *Journal of Cosmology and Astroparticle Physics* **2019** (11), 043–043.
- [49] D. N. Limber, The Analysis of Counts of the Extragalactic Nebulae in Terms of a Fluctuating Density Field. II., *Astrophys. J.* **119**, 655 (1954).
- [50] S. Bridle and L. King, Dark energy constraints from cosmic shear power spectra: impact of intrinsic alignments on photometric redshift requirements, *New Journal of Physics* **9**, 444 (2007), [arXiv:0705.0166 \[astro-ph\]](#).
- [51] M. A. Troxel, N. MacCrann, J. Zuntz, T. F. Eifler, E. Krause, S. Dodelson, D. Gruen, J. Blazek, O. Friedrich, S. Samuroff, J. Prat, L. F. Secco, C. Davis, A. Ferté, J. DeRose, A. Alarcon, A. Amara, E. Baxter, M. R. Becker, G. M. Bernstein, S. L. Bridle, R. Cawthon, C. Chang, A. Choi, J. De Vicente, A. Drlica-Wagner, J. Elvin-Poole, J. Frieman, M. Gatti, W. G. Hartley,

- K. Honscheid, B. Hoyle, E. M. Huff, D. Huterer, B. Jain, M. Jarvis, T. Kacprzak, D. Kirk, N. Kokron, C. Krawiec, O. Lahav, A. R. Liddle, J. Peacock, M. M. Rau, A. Refregier, R. P. Rollins, E. Roza, E. S. Rykoff, C. Sánchez, I. Sevilla-Noarbe, E. Sheldon, A. Stebbins, T. N. Varga, P. Vielzeuf, M. Wang, R. H. Wechsler, B. Yanny, T. M. C. Abbott, F. B. Abdalla, S. Allam, J. Annis, K. Bechtol, A. Benoit-Lévy, E. Bertin, D. Brooks, E. Buckley-Geer, D. L. Burke, A. Carnero Rosell, M. Carrasco Kind, J. Carretero, F. J. Castander, M. Crocce, C. E. Cunha, C. B. D'Andrea, L. N. da Costa, D. L. DePoy, S. Desai, H. T. Diehl, J. P. Dietrich, P. Doel, E. Fernandez, B. Flaugher, P. Fosalba, J. García-Bellido, E. Gaztanaga, D. W. Gerdes, T. Giannantonio, D. A. Goldstein, R. A. Gruendl, J. Gschwend, G. Gutierrez, D. J. James, T. Jeltema, M. W. G. Johnson, M. D. Johnson, S. Kent, K. Kuehn, S. Kuhlmann, N. Kuropatkin, T. S. Li, M. Lima, H. Lin, M. A. G. Maia, M. March, J. L. Marshall, P. Martini, P. Melchior, F. Menanteau, R. Miquel, J. J. Mohr, E. Neilsen, R. C. Nichol, B. Nord, D. Petravick, A. A. Plazas, A. K. Romer, A. Roodman, M. Sako, E. Sanchez, V. Scarpine, R. Schindler, M. Schubnell, M. Smith, R. C. Smith, M. Soares-Santos, F. Sobreira, E. Suchyta, M. E. C. Swanson, G. Tarle, D. Thomas, D. L. Tucker, V. Vikram, A. R. Walker, J. Weller, Y. Zhang, and DES Collaboration, Dark Energy Survey Year 1 results: Cosmological constraints from cosmic shear, *Phys. Rev. D* **98**, 043528 (2018), [arXiv:1708.01538 \[astro-ph.CO\]](#).
- [52] D. Alonso, J. Sanchez, and A. Slosar, A unified pseudo-cl framework, *MNRAS* **484**, 4127–4151 (2019).
- [53] D. Enard, The ESO Very Large Telescope project - Present status, in *Advanced technology optical telescopes III*, Society of Photo-Optical Instrumentation Engineers (SPIE) Conference Series, Vol. 628, edited by L. D. Barr (1986) pp. 221–226.
- [54] M. Capaccioli, D. Mancini, and G. Sedmak, The VLT Survey Telescope: A Status Report, *The Messenger* **120**, 10 (2005).
- [55] J. P. Emerson and W. J. Sutherland, VISTA: status and performance, in *Ground-based and Airborne Telescopes III*, Society of Photo-Optical Instrumentation Engineers (SPIE) Conference Series, Vol. 7733, edited by L. M. Stepp, R. Gilmozzi, and H. J. Hall (2010) p. 773306.
- [56] W. Sutherland, J. Emerson, G. Dalton, E. Atad-Etchedgui, S. Beard, R. Bennett, N. Bezawada, A. Born, M. Caldwell, P. Clark, S. Craig, D. Henry, P. Jeffers, B. Little, A. McPherson, J. Murray, M. Stewart, B. Stobie, D. Terrett, K. Ward, M. Whalley, and G. Woodhouse, The Visible and Infrared Survey Telescope for Astronomy (VISTA): Design, technical overview, and performance, *Astronomy & Astrophysics* **575**, A25 (2015), [arXiv:1409.4780 \[astro-ph.IM\]](#).
- [57] K. Kuijken, C. Heymans, A. Dvornik, H. Hildebrandt, J. T. A. de Jong, A. H. Wright, T. Erben, M. Bilicki, B. Giblin, H.-Y. Shan, F. Getman, A. Grado, H. Hoekstra, L. Miller, N. Napolitano, M. Paolilo, M. Radovich, P. Schneider, W. Sutherland, M. Tewes, C. Tortora, E. A. Valentijn, and G. A. Verdoes Kleijn, The fourth data release of the Kilo-Degree Survey: ugri imaging and nine-band optical-IR photometry over 1000 square degrees, *Astronomy & Astrophysics* **625**, A2 (2019), [arXiv:1902.11265 \[astro-ph.GA\]](#).
- [58] B. Giblin, C. Heymans, M. Asgari, H. Hildebrandt, H. Hoekstra, B. Joachimi, A. Kannawadi, K. Kuijken, C.-A. Lin, L. Miller, T. Tröster, J. L. van den Busch, A. H. Wright, M. Bilicki, C. Blake, J. de Jong, A. Dvornik, T. Erben, F. Getman, N. R. Napolitano, P. Schneider, H. Shan, and E. Valentijn, KiDS-1000 catalogue: Weak gravitational lensing shear measurements, *Astronomy & Astrophysics* **645**, A105 (2021), [arXiv:2007.01845 \[astro-ph.CO\]](#).
- [59] A. Edge, W. Sutherland, K. Kuijken, S. Driver, R. McMahon, S. Eales, and J. P. Emerson, The VISTA Kilo-degree Infrared Galaxy (VIKING) Survey: Bridging the Gap between Low and High Redshift, *The Messenger* **154**, 32 (2013).
- [60] D. G. York, J. Adelman, J. E. Anderson, Jr., S. F. Anderson, J. Annis, N. A. Bahcall, J. A. Bakken, R. Barkhouser, S. Bastian, E. Berman, W. N. Boroski, S. Bracker, C. Briegel, J. W. Briggs, J. Brinkmann, R. Brunner, S. Burles, L. Carey, M. A. Carr, F. J. Castander, B. Chen, P. L. Colestock, A. J. Connolly, J. H. Crocker, I. Csabai, P. C. Czarapata, J. E. Davis, M. Doi, T. Dombeck, D. Eisenstein, N. Ellman, B. R. Elms, M. L. Evans, X. Fan, G. R. Federwitz, L. Fiscelli, S. Friedman, J. A. Frieman, M. Fukugita, B. Gillespie, J. E. Gunn, V. K. Gurbani, E. de Haas, M. Haldeman, F. H. Harris, J. Hayes, T. M. Heckman, G. S. Hennessy, R. B. Hindsley, S. Holm, D. J. Holmgren, C.-h. Huang, C. Hull, D. Husby, S.-I. Ichikawa, T. Ichikawa, Ž. Ivezić, S. Kent, R. S. J. Kim, E. Kinney, M. Klaene, A. N. Kleinman, S. Kleinman, G. R. Knapp, J. Korienek, R. G. Kron, P. Z. Kunszt, D. Q. Lamb, B. Lee, R. F. Leger, S. Limmongkol, C. Lindenmeyer, D. C. Long, C. Loomis, J. Loveday, R. Lucinio, R. H. Lupton, B. MacGinnon, E. J. Mannery, P. M. Mantsch, B. Margon, P. McKee, T. A. McKay, A. Meiksin, A. Merelli, D. G. Monet, J. A. Munn, V. K. Narayanan, T. Nash, E. Neilsen, R. Neswold, H. J. Newberg, R. C. Nichol, T. Nicinski, M. Nonino, N. Okada, S. Okamura, J. P. Ostriker, R. Owen, A. G. Pauls, J. Peoples, R. L. Peterson, D. Petravick, J. R. Pier, A. Pope, R. Pordes, A. Prosapio, R. Rechenmacher, T. R. Quinn, G. T. Richards, M. W. Richmond, C. H. Rivetta, C. M. Rockosi, K. Ruthmansdorfer, D. Sandford, D. J. Schlegel, D. P. Schneider, M. Sekiguchi, G. Sergey, K. Shimasaku, W. A. Siegmund, S. Smee, J. A. Smith, S. Snedden, R. Stone, C. Stoughton, M. A. Strauss, C. Stubbs, M. SubbaRao, A. S. Szalay, I. Szapudi, G. P. Szokoly, A. R. Thakar, C. Tremonti, D. L. Tucker, A. Uomoto, D. Vanden Berk, M. S. Vogeley, P. Waddell, S.-i. Wang, M. Watanabe, D. H. Weinberg, B. Yanny, N. Yasuda, and SDSS Collaboration, The Sloan Digital Sky Survey: Technical Summary, *AJ* **120**, 1579 (2000), [arXiv:astro-ph/0006396 \[astro-ph\]](#).
- [61] C. Blake, S. Brough, W. Couch, K. Glazebrook, G. Poole, T. Davis, M. Drinkwater, R. Jurek, K. Pimblet, M. Colless, R. Sharp, S. Croom, M. Pracy, D. Woods, B. Madore, C. Martin, and T. Wyder, The WiggleZ Dark Energy Survey, *Astronomy and Geophysics* **49**, 5.19 (2008).
- [62] C. Blake, A. Amon, M. Childress, T. Erben, K. Glazebrook, J. Harnois-Deraps, C. Heymans, H. Hildebrandt, S. R. Hinton, S. Janssens, A. Johnson, S. Joudaki, D. Klaes, K. Kuijken, C. Lidman, F. A. Marin, D. Parkinson, G. B. Poole, and C. Wolf, The 2-degree Field Lensing Survey: design and clustering measurements, *MNRAS* **462**, 4240 (2016), [arXiv:1608.02668 \[astro-ph.CO\]](#).

- [63] DESI Collaboration, B. Abareshi, J. Aguilar, S. Ahlen, S. Alam, D. M. Alexander, R. Alfarsy, L. Allen, C. Allende Prieto, O. Alves, J. Ameel, E. Armengaud, J. Asorey, A. Aviles, S. Bailey, A. Balaguera-Antolínez, O. Ballester, C. Baltay, A. Bault, S. F. Beltran, B. Benavides, S. BenZvi, A. Berti, R. Besuner, F. Beutler, D. Bianchi, C. Blake, P. Blanc, R. Blum, A. Bolton, S. Bose, D. Bramall, S. Brieden, A. Brodzeller, D. Brooks, C. Brownell, E. Buckley-Geer, R. N. Cahn, Z. Cai, R. Canning, R. Capasso, A. Carnero Rosell, P. Carton, R. Casas, F. J. Castander, J. L. Cervantes-Cota, S. Chabanier, E. Chaussidon, C. Chuang, C. Circosta, S. Cole, A. P. Cooper, L. da Costa, M.-C. Cousinou, A. Cuceu, T. M. Davis, K. Dawson, R. de la Cruz-Noriega, A. de la Macorra, A. de Mattia, J. Della Costa, P. Demmer, M. Derwent, A. Dey, B. Dey, G. Dhungana, Z. Ding, C. Dobson, P. Doel, J. Donald-McCann, J. Donaldson, K. Douglass, Y. Duan, P. Dunlop, J. Edelman, S. Eftekharzadeh, D. J. Eisenstein, M. Enriquez-Vargas, S. Escoffier, M. Evatt, P. Fagrellius, X. Fan, K. Fanning, V. A. Fawcett, S. Ferraro, J. Ereza, B. Flaugher, A. Font-Ribera, J. E. Forero-Romero, C. S. Frenk, S. Fromenteau, B. T. Gänsicke, C. Garcia-Quintero, L. Garrison, E. Gaztañaga, F. Gerardi, H. Gil-Marín, S. Gontcho A Gontcho, A. X. Gonzalez-Morales, G. Gonzalez-de-Rivera, V. Gonzalez-Perez, C. Gordon, O. Graur, D. Green, C. Grove, D. Gruen, G. Gutierrez, J. Guy, C. Hahn, S. Harris, D. Herrera, H. K. Herrera-Alcantar, K. Honscheid, C. Howlett, D. Huterer, V. Iršič, M. Ishak, P. Jelinsky, L. Jiang, J. Jimenez, Y. P. Jing, R. Joyce, E. Jullo, S. Juneau, N. G. Karaçaylı, M. Karamanis, A. Karcher, T. Karim, R. Kehoe, S. Kent, D. Kirkby, T. Kisner, F. Kitaura, S. E. Kopusov, A. Kovács, A. Kremin, A. Krolewski, B. L’Huillier, O. Lahav, A. Lambert, C. Lamman, T.-W. Lan, M. Landriau, S. Lane, D. Lang, J. U. Lange, J. Lasker, L. Le Guillou, A. Leauthaud, A. Le Van Suu, M. E. Levi, T. S. Li, C. Magneville, M. Manera, C. J. Manser, B. Marshall, P. Martini, W. McCollam, P. McDonald, A. M. Meisner, J. Mena-Fernández, J. Meneses-Rizo, M. Mezcua, T. Miller, R. Miquel, P. Montero-Camacho, J. Moon, J. Moustakas, E. Mueller, A. Muñoz-Gutiérrez, A. D. Myers, S. Nadathur, J. Najita, L. Napolitano, E. Neilsen, J. A. Newman, J. D. Nie, Y. Ning, G. Niz, P. Norberg, H. E. Noriega, T. O’Brien, A. Obuljen, N. Palanque-Delabrouille, A. Palmese, P. Zhiwei, D. Pappalardo, X. PENG, W. J. Percival, S. Perruchot, R. Pogge, C. Poppett, A. Porredon, F. Prada, J. Prochaska, R. Pucha, A. Pérez-Fernández, I. Pérez-Ràfols, D. Rabinowitz, and A. Raichoor, Overview of the Instrumentation for the Dark Energy Spectroscopic Instrument, *AJ* **164**, 207 (2022), [arXiv:2205.10939 \[astro-ph.IM\]](#).
- [64] S. P. Driver, S. Bellstedt, A. S. G. Robotham, I. K. Baldry, L. J. Davies, J. Liske, D. Obreschkow, E. N. Taylor, A. H. Wright, M. Alpaslan, S. P. Bamford, A. E. Bauer, J. Bland-Hawthorn, M. Bilicki, M. Bravo, S. Brough, S. Casura, M. E. Cluver, M. Colless, C. J. Conselice, S. M. Croom, J. de Jong, F. D’Eugenio, R. De Propriis, B. Dogruel, M. J. Drinkwater, A. Dvornik, D. J. Farrow, C. S. Frenk, B. Giblin, A. W. Graham, M. W. Grootes, M. L. P. Gunawardhana, A. Hashemizadeh, B. Häußler, C. Heymans, H. Hildebrandt, B. W. Holwerda, A. M. Hopkins, T. H. Jarrett, D. Heath Jones, L. S. Kelvin, S. Koushan, K. Kuijken, M. A. Lara-López, R. Lange, Á. R. López-Sánchez, J. Loveday, S. Mahajan, M. Meyer, A. J. Moffett, N. R. Napolitano, P. Norberg, M. S. Owers, M. Radovich, M. Raouf, J. A. Peacock, S. Phillipps, K. A. Pimbblet, C. Popescu, K. Said, A. E. Sansom, M. Seibert, W. J. Sutherland, J. E. Thorne, R. J. Tuffs, R. Turner, A. van der Wel, E. van Kampen, and S. M. Wilkins, Galaxy And Mass Assembly (GAMA): Data Release 4 and the $z < 0.1$ total and $z < 0.08$ morphological galaxy stellar mass functions, *MNRAS* **513**, 439 (2022), [arXiv:2203.08539 \[astro-ph.GA\]](#).
- [65] N. Benítez, Bayesian Photometric Redshift Estimation, *Astrophys. J.* **536**, 571 (2000), [arXiv:astro-ph/9811189 \[astro-ph\]](#).
- [66] T. Kohonen, *Self-Organizing Maps* (Springer series in information sciences, 2001, xx, 501, 2001).
- [67] J. E. Geach, Unsupervised self-organized mapping: a versatile empirical tool for object selection, classification and redshift estimation in large surveys, *MNRAS* **419**, 2633 (2012), [arXiv:1110.0005 \[astro-ph.IM\]](#).
- [68] A. H. Wright, H. Hildebrandt, J. L. van den Busch, C. Heymans, B. Joachimi, A. Kannawadi, and K. Kuijken, KiDS+VIKING-450: Improved cosmological parameter constraints from redshift calibration with self-organising maps, *Astronomy & Astrophysics* **640**, L14 (2020), [arXiv:2005.04207 \[astro-ph.CO\]](#).
- [69] K. M. Gorski, E. Hivon, A. J. Banday, B. D. Wandelt, F. K. Hansen, M. Reinecke, and M. Bartelmann, Healpix: A framework for high-resolution discretization and fast analysis of data distributed on the sphere, *The Astrophysical Journal* **622**, 759–771 (2005).
- [70] A. Nicola, C. García-García, D. Alonso, J. Dunkley, P. G. Ferreira, A. Slosar, and D. N. Spergel, Cosmic shear power spectra in practice, *Journal of Cosmology and Astroparticle Physics* **2021** (03), 067.
- [71] N. E. Chisari, D. Alonso, E. Krause, C. D. Leonard, P. Bull, J. Neveu, A. S. Villarreal, S. Singh, T. McClintock, J. Ellison, Z. Du, J. Zuntz, A. Mead, S. Joudaki, C. S. Lorenz, T. Tröster, J. Sanchez, F. Lanusse, M. Ishak, R. Hlozek, J. Blazek, J.-E. Campagne, H. Almoubayyed, T. Eifler, M. Kirby, D. Kirkby, S. Plaszczynski, A. Slosar, M. Vrástil, E. L. Wagoner, and LSST Dark Energy Science Collaboration, Core Cosmology Library: Precision Cosmological Predictions for LSST, *ApJ Supp.* **242**, 2 (2019), [arXiv:1812.05995 \[astro-ph.CO\]](#).
- [72] R. Reischke, S. Unruh, M. Asgari, A. Dvornik, H. Hildebrandt, B. Joachimi, L. Porth, M. von Wietersheim-Kramsta, J. L. van den Busch, B. Stözlner, A. H. Wright, Z. Yan, M. Bilicki, P. Burger, J. Harnois-Deraps, C. Georgiou, C. Heymans, P. Jalan, S. Joudaki, K. Kuijken, S.-S. Li, L. Linke, C. Mahony, D. Sciotti, and T. Tröster, KiDS-Legacy: Covariance validation and the unified OneCovariance framework for projected large-scale structure observables, [arXiv e-prints](#), [arXiv:2410.06962](#) (2024), [arXiv:2410.06962 \[astro-ph.CO\]](#).
- [73] The LSST Dark Energy Science Collaboration, R. Mandelbaum, T. Eifler, R. Hlozek, T. Collett, E. Gawiser, D. Scolnic, D. Alonso, H. Awan, R. Biswas, J. Blazek, P. Burchat, N. E. Chisari, I. Dell’Antonio, S. Digel, J. Frieman, D. A. Goldstein, I. Hook, Ž. Ivezić, S. M. Kahn, S. Kamath, D. Kirkby, T. Kitching, E. Krause, P.-F. Leget, P. J. Marshall, J. Meyers, H. Miyatake, J. A. Newman, R. Nichol, E. Rykoff, F. J. Sanchez,

- A. Slosar, M. Sullivan, and M. A. Troxel, The LSST Dark Energy Science Collaboration (DESC) Science Requirements Document, [arXiv e-prints](#) , [arXiv:1809.01669 \(2018\)](#), [arXiv:1809.01669 \[astro-ph.CO\]](#).
- [74] J. U. Lange, Nautilus: A High-Efficiency Bayesian Sampler for Astronomy, in *American Astronomical Society Meeting Abstracts*, American Astronomical Society Meeting Abstracts, Vol. 244 (2024) p. 229.02.
- [75] https://github.com/ShimingGu/BNT_PRD/.
- [76] A. Lewis, GetDist: a Python package for analysing Monte Carlo samples, [arXiv e-prints](#) , [arXiv:1910.13970 \(2019\)](#), [arXiv:1910.13970 \[astro-ph.IM\]](#).